

Influences of local and remote conditions on tropical precipitation and its response to climate change

Article

Accepted Version

Saint-Lu, M., Chadwick, R., Lambert, F. H., Collins, M., Boutle, I., Whittall, M. and Daleu, C. (2020) Influences of local and remote conditions on tropical precipitation and its response to climate change. *Journal of Climate*, 33 (10). pp. 4045-4063. ISSN 1520-0442 doi: <https://doi.org/10.1175/JCLI-D-19-0450.1> Available at <https://centaur.reading.ac.uk/89284/>

It is advisable to refer to the publisher's version if you intend to cite from the work. See [Guidance on citing](#).

To link to this article DOI: <http://dx.doi.org/10.1175/JCLI-D-19-0450.1>

Publisher: American Meteorological Society

All outputs in CentAUR are protected by Intellectual Property Rights law, including copyright law. Copyright and IPR is retained by the creators or other copyright holders. Terms and conditions for use of this material are defined in the [End User Agreement](#).

www.reading.ac.uk/centaur

CentAUR

Central Archive at the University of Reading

Reading's research outputs online

1 **Influences of local and remote conditions on tropical precipitation**
2 **and its response to climate change**

3 Marion Saint-Lu^{*†}

4 *University of Exeter, Exeter, United Kingdom*

5 Robin Chadwick

6 *Met Office Hadley Centre, and Global Systems Institute, University of Exeter, Exeter, UK*

7 F. Hugo Lambert

8 *University of Exeter, Exeter, UK*

9 Matthew Collins

10 *University of Exeter, Exeter, UK*

11 Ian Boutle

12 *Met Office, Exeter, UK*

13 Michael Whittall

14 *Met Office, Exeter, UK*

15 Chimene Daleu

16 *University of Reading, Reading, UK*

¹⁷ **Corresponding author address:* LMD/IPSL, UPMC boite 99, 4 place Jussieu, 75252 Paris Cedex
¹⁸ 05, France.

¹⁹ E-mail: marion.saint-lu@lmd.jussieu.fr

²⁰ [†]Current Affiliation: Laboratoire de Météorologie Dynamique (LMD) / Institut Pierre Simon
²¹ Laplace (IPSL), Sorbonne Université, Université Pierre et Marie Curie, Paris, France.

ABSTRACT

22 By comparing a Single Column Model (SCM) with closely related Gen-
23 eral Circulation Models (GCMs), precipitation changes that can be diagnosed
24 from local changes in surface temperature (T_S) and relative humidity (RH_S)
25 are separated from more complex responses. In the SCM set-up, the large-
26 scale tropical circulation is parametrized to respond to the surface temperature
27 departure from a prescribed environment, following the Weak Temperature
28 Gradient (WTG) approximation and using the Damped Gravity Wave (DGW)
29 parametrization. The SCM is also forced with moisture variations. First, it
30 is found that most of the present-day mean tropical rainfall and circulation
31 pattern is associated with T_S and RH_S patterns. Climate change experiments
32 with the SCM are performed, imposing separately surface warming and CO_2
33 increase. The rainfall response to future changes in sea surface temperature
34 patterns and plant physiology are successfully reproduced, suggesting that
35 these are direct responses to local changes in convective instability. How-
36 ever, the SCM increases oceanic rainfall too much, and fails to reproduce
37 the land rainfall decrease, that are both associated with uniform ocean warm-
38 ing. It is argued that remote atmospheric teleconnections play a crucial role in
39 both weakening the atmospheric overturning circulation and constraining pre-
40 cipitation changes. Results suggest that the overturning circulation weakens,
41 both as a direct local response to increased CO_2 and in response to energy-
42 imbalance driven exchanges between ascent and descent regions.

43 1. Introduction

44 Uncertainty remains in how tropical rainfall will change in the future, particularly at regional
45 scales. Previous studies have shown that the mean future changes in tropical rainfall mainly consist
46 in shifts, which over the oceans are mainly driven by changes in the mean Sea Surface Temperature
47 (SST) pattern, following the so-called warmer-get-wetter mechanism (Xie et al. 2010; Ma and Xie
48 2013; Chadwick et al. 2014; Kent et al. 2015). However, rainfall changes over land seem to be
49 driven by more complex combinations of different aspects of the CO₂ forcing, including changes
50 in the plant physiology, in the atmospheric radiative cooling or in the mean ocean warming (e.g.
51 Betts et al. 2004; Giannini 2010; Cao et al. 2012; Chadwick et al. 2017). Understanding tropical
52 rainfall changes under global warming would help to improve future projections that still exhibit
53 strong disagreement and better inform climate adaptation policy (Knutti and Sedlek 2013; Collins
54 et al. 2013; Shepherd 2014; Kent et al. 2015; Oueslati et al. 2016; Long et al. 2016).

55 Based on the observation that horizontal gradients of free-tropospheric temperatures are weak
56 in the Tropics, the so-called Weak Temperature Gradient (WTG) approximation suggests that con-
57 vective instability is largely driven by spatial variations in surface temperature and moisture (Sobel
58 and Bretherton 2000; Sobel et al. 2001). The influence of free-tropospheric moisture gradients on
59 precipitation patterns is not ruled out by the WTG approximation.

60 Based on this theory, Lambert et al. (2017) and Todd et al. (2018) have diagnosed tropical
61 rainfall patterns and shifts from two surface observable variables, surface Temperature (T_S) and
62 near-surface Relative Humidity (RH_S), with the idea that precipitation falls in the highest T_S and
63 RH_S regions. This view is based on the argument (from convective quasi-equilibrium and WTG
64 approximation) that tropical precipitation is a function of T_S and RH_S and that rainfall shifts can
65 be diagnosed from the combination of T_S shifts and RH_S shifts.

66 The general aim of this study is to test how much of the pattern of mean tropical precipitation
 67 and its response to climate change can be simulated from T_S and RH_S patterns using a Single
 68 Column Model (SCM) under the WTG approximation. This study first investigates how much of
 69 the present-day annual-mean tropical rainfall pattern simulated by a General Circulation Model
 70 (GCM) can be reproduced by reconstructing only three elements: 1) the environment provided
 71 by the tropical mean-state, 2) the T_S tropical pattern, 3) the RH_S tropical pattern. Simulating a
 72 single atmospheric column, embedded in a pre-determined environment, allows us to reconstruct
 73 those three elements since the only information needed is: 1) the moisture and temperature pro-
 74 files that describe the tropical environment, 2) the local T_S anomaly at each location (departure
 75 from the environment), 3) the local RH_S at each location. We use an SCM modified to imple-
 76 ment the WTG approximation, so that precipitation in the column responds to the T_S anomaly via
 77 the parametrization of the large-scale circulation. The latter is done using the so-called Damped
 78 Gravity Wave (DGW) parametrization method (Bergman and Sardeshmukh 2004; Kuang 2008,
 79 2011; Wang et al. 2013) and has been implemented following Daleu et al. (2015). Similar set-ups
 80 have been used in many studies (e.g. Sobel and Bretherton 2000; Chiang and Sobel 2002; Sobel
 81 et al. 2007; Sobel and Bellon 2009; Zhu and Sobel 2012). In addition, we implement the variation
 82 of moisture in the column in order to represent the precipitation response to RH_S . The SCM is
 83 run multiple times to reconstruct the tropical T_S and RH_S patterns from the corresponding parent
 84 GCM. The rainfall pattern reproduced from this reconstruction is then compared with the GCM.
 85 The experimental set-up is described in detail in Section 2.

86 In the second part of the study, increased atmospheric CO_2 and uniform surface warming are
 87 independently applied to the SCM in order to investigate how much of the rainfall response can
 88 be reproduced by reconstructing: 1) the change in the tropical mean-state environment, 2) the
 89 change in the T_S tropical pattern, 3) the change in the RH_S tropical pattern. Those three compo-

nents are reconstructed for different aspects of CO₂ forcing, such as uniform ocean warming, SST pattern change or direct radiative effect of increased atmospheric CO₂. They are taken from GCM atmosphere-only experiments in which these boundary conditions have been applied. Rainfall changes reproduced from these reconstructions in the SCM are then compared to the corresponding GCM experiment.

In addition to rainfall, we also investigate changes in convective mass fluxes which can be used as a proxy for the intensity of the atmospheric circulation. Precipitation can be approximated as the product of near-surface specific humidity and vertically integrated convective mass flux. In a warmer and wetter climate, rainfall can increase even as convective mass flux decreases (Held and Soden 2006). Convective mass flux is expected to weaken in response to climate change, which has been attributed to the reduction of radiative cooling, or the enhanced warming of the subtropics, or the increase in dry static stability as a response to surface warming (e.g. Knutson and Manabe 1995; Held and Soden 2006; Vecchi and Soden 2007; Ma et al. 2012; Chadwick et al. 2013; Bony et al. 2013; He et al. 2014; He and Soden 2015). In order to test these mechanisms in the SCM, we use a more direct approach where we look at the direct response of the column to the forcing, without reconstructing RH_S patterns changes from the GCM. This way, we use the SCM to further understand whether the tropical circulation weakening is a direct or indirect, uniform or non-uniform response to increased atmospheric CO₂. The weakening of the tropical circulation further affects the rainfall changes, which are also investigated.

2. SCM description and set-up

The SCM uses the Met Office Unified Model Global Atmosphere version 7.1 in one dimension, which is also used in three dimensions in the atmosphere-only GCM HadGEM3 (Walters et al. 2019). The surface is prescribed, with no ocean or land-surface model. The SCM has interac-

113 tive radiation and solar diurnal cycle. There is no surface temperature variability applied on any
114 timescale.

115 *a. Parametrization of the large-scale circulation in the SCM*

116 Conceptually, the SCM represents two atmospheric domains: the simulated column and a pre-
117 scribed environment that typically represents the tropical mean. The environment is defined by
118 reference vertical profiles of potential temperature θ and specific humidity q . In order to de-
119 termine these profiles, the SCM is first run in Radiative-Convective Equilibrium (RCE) mode:
120 vertical velocity is set to zero so that convective heating balances radiative cooling. Surface tem-
121 perature is prescribed and represents the tropical average SST. Reference profiles of θ and q are
122 determined from the equilibrated state of the RCE run. They will constitute the environment and
123 initial state for DGW-parametrized SCM simulations, described below, with their mathematical
124 framework detailed in appendix A.

125 In the single column simulated using the DGW parametrization, the prescribed surface tempera-
126 ture affects the column stability (compared to the initial state/environment), which in turns affects
127 convection and convective heating, warming or cooling the column. The column is also warmed
128 or cooled by changes in the sensible heat flux and in water vapour and clouds which then feed
129 back on the column radiative heating. The vertical velocity w' , that is the marker of the large-scale
130 circulation in the column, is parametrized to respond to the column temperature anomaly. The
131 subsequent vertical advection of θ relaxes the simulated θ profile towards the reference θ profile,
132 maintaining approximate uniformity with the environment, as dictated by the WTG approxima-
133 tion (see schematic Fig. 1). Together with the subsequent vertical advection of q , it further affects
134 rainfall.

135 Another method commonly used is the WTG parametrization (Sobel and Bretherton 2000; Sobel
136 et al. 2001), that is only used here in the Supplementary Material. Note that both the DGW and
137 the WTG parametrization methods follow the WTG approximation. The DGW parametrization
138 of w' , unlike the WTG parametrization, takes place in the whole column, including the boundary
139 layer, without linear interpolation.

140 This SCM set-up represents the local effect of T_S patterns on convective instability and thus free-
141 tropospheric latent heating, which then drives low-level convergence (represented by the vertical
142 velocity in the SCM) and convection. On the other hand, our SCM set-up is not representative of
143 the Lindzen and Nigam (1987) model, which describes the more direct effect of sharp T_S gradients
144 on low-level convergence via their influence on boundary layer pressure gradients. The SCM
145 parametrization represents the effect of the T_S anomaly regarding the tropical average, but is not
146 able to simulate sharp T_S gradients.

147 Horizontal advection of moisture between the environment and the simulated domain is mod-
148 elled using simultaneously two different schemes that represent two different processes: (1) the
149 horizontal advection by the locally parametrized mean divergent circulation (lateral drawing), (2)
150 the horizontal advection by the mean rotational flow and transient eddies in the form of a relaxation
151 of the domain q profile towards the environmental q profile (moisture relaxation). The time-scale
152 used for this relaxation is 1 day, which would be typical of horizontal moisture mixing between the
153 simulated domain and a surrounding environment that is far enough away to be independent of the
154 former. More details and mathematical formulation of the DGW parametrization and horizontal
155 advection of moisture are given in appendix A.

156 *b. Varying moisture in the SCM*

157 During a further stage of this study, in order to include variations of moisture and to be able to
158 produce various values of RH_S (particularly low values found over land), we add to this set-up a
159 scaling of both surface evaporation (with a coefficient β) and environmental q profile. The envi-
160 ronmental q profile is scaled with the same coefficient throughout the whole column. We use a
161 range of combinations of those two scaling coefficients for each surface temperature. This allows
162 us to vary moisture in the column, which also affects precipitation. It also allows us to have a better
163 representation of the different tropical regions since there is no weak moisture gradient principle
164 in the tropics. The β and q profile scaling coefficients are determined by spatial clustering anal-
165 yses (see section 1 of Supplementary material). Following these analyses, surface evaporation is
166 varied using 5 coefficients that represent: (1) the ocean ($\beta=1$), (2) rainforests ($\beta=0.75$), (3) a 20%
167 reduction of the evaporation over rainforests as is expected in response to $4\times\text{CO}_2$ increase (our
168 vegetation-only forcing component with prescribed land gives a 17% reduction over rainforests
169 latitudes over land) ($\beta=0.6$), (4) wet regions ($\beta=0.5$), (5) semi-arid regions ($\beta=0.2$). The environ-
170 mental q profile is varied using 7 coefficients that represent: heavy rainfall convergence zones and
171 rainforests (scaling coefficient = 1 and 1.1), north and south subtropics (0.8 and 0.7), north and
172 south equatorial bands (1 and 0.9), deserts (0.4) and the Amazon during wet season (1.25).

173 *c. Experimental design*

174 First, the SCM is run in RCE mode in order to determine the environment. Atmospheric CO_2
175 concentrations are set to mid-1970s values. The run is performed for 100 days at $T_s^{RCE} = 300$ K,
176 which is approximately the mean SST over the tropics (20N-20S). Reference θ and q profiles are
177 determined from the time-mean over the last 40 days of the RCE run. These profiles are then used
178 as initial state and environment in the SCM runs under the DGW parametrization.

179 In the first stage of this study, the SCM is run 13 times under the DGW parametrization, with
180 the surface temperature varying from 297.5 to 303.5 K, in increments of 0.5 K (β and the environ-
181 mental q profile scaling coefficients are both set to 1). This set of experiments will be referred to
182 as SCM_CTRL- T_S -only.

183 During a further stage of this study, the SCM is run multiple times with many possible com-
184 binations of T_S , β and environmental q profile scaling. In total a set of 455 ($13 T_S \times 5 \beta \times 7 q$
185 scalings) SCM experiments are run to cover enough possibilities of T_S , RH_S and rainfall conditions
186 in the column in order to reproduce rainfall patterns. We will refer to this set of experiments as
187 SCM_CTRL.

188 In the last stage of this study, the set of 455 SCM experiments is replicated twice with two
189 different perturbations. The control set of experiments mentioned above (SCM_CTRL) serves as
190 the reference. A first set of perturbed experiments is performed with warmer mean conditions
191 corresponding to a uniform warming of the surface by 4 K (SCM_4K). For this set of experiments,
192 the SCM is first run in RCE mode at $T_s^{RCE} = 304$ K. Again, this run is performed for 100 days
193 and the new reference θ and q profiles are determined from the time-mean over the last 40 days.
194 These new profiles are then used as initial state and environment to perform a new set of runs
195 under the DGW parametrization: the SCM is run again 455 times, varying T_S from 301.5 to
196 307.5 K every 0.5 K, and varying moisture using the same β and q profile scaling coefficients as in
197 SCM_CTRL. A second set of perturbed experiments is performed with increased atmospheric CO_2
198 corresponding to the $4 \times \text{CO}_2$ forcing (SCM_4xCO2). For this set of experiments, the SCM is first
199 run in RCE mode again at $T_s^{RCE} = 300$ K as in SCM_CTRL, but with atmospheric CO_2 multiplied
200 by 4. As before, the run is performed for 100 days, the new reference profiles are determined from
201 the time-mean over the last 40 days and then used as initial state and environment to perform a

new set of runs under the DGW parametrization: the SCM is run again 455 times, varying T_S , β and the q profile scaling as in SCM_CTRL but with 4 times more CO₂ in the atmospheric column.

3. GCM experiments

Different experiments from different GCMs are compared with the SCM results. They are all described in Table 1. The most relevant comparison is with the atmosphere-only experiment AMIP (Atmospheric Modelling Intercomparison Project) performed with the SCM’s parent GCM HadGEM3 (Walters et al. 2019). We consider 20 years of this experiment from 1989 to 2008 and refer to it as HG3-AMIP. In HG3-AMIP, prescribed SST is taken from observations.

In order to investigate the response to the $4\times\text{CO}_2$ forcing, we compare the pre-industrial (pi-Control) and abrupt $4\times\text{CO}_2$ simulations performed with the previous version of the Met Office Unified Model HadGEM2-ES (Martin et al. 2011). In order to decompose the $4\times\text{CO}_2$ forcing, we use atmosphere-only experiments, each perturbed with one isolated component of the forcing (Table 1). Some of them have been performed with HadGEM2-ES and are described in more detail in Chadwick et al. (2017) (piSST, p4KSST, a4SST). At the time of writing, none of these experiments have been performed with HadGEM3 (the SCM’s parent GCM); HadGEM2-ES was then most likely the closest model to be compared to the SCM. The other atmosphere-only experiments used in this study have prescribed land in addition to prescribed ocean. They have only been performed with ACCESS1.0 (Bi et al. 2013; Ackerley and Dommenges 2016) and are described in more detail in Ackerley et al. (2018). ACCESS1.0 and HadGEM2-ES are very similar models sharing the same configurations of their land-surface and atmospheric components (including convection scheme). Using these “prescribed-land” experiments allows us to decompose the $4\times\text{CO}_2$ forcing more, since land-surface changes are separated from ocean-surface changes.

For all these GCM experiments, the last 30 years are considered. The different components of the $4\times\text{CO}_2$ forcing built from combinations of these experiments are defined in Table 2. The Vegetation-only forcing with prescribed land shows the effect of the plant physiological response to $4\times\text{CO}_2$ with prescribed surface temperature over land and ocean. The $4\times\text{CO}_2$ radiative-only forcing with prescribed land shows the $4\times\text{CO}_2$ radiative-only effect (no plant physiology change) with prescribed surface temperature over land and ocean. Other definitions given in Table 2 are self-explanatory.

4. Present-day climate

a. Reproduction from surface temperature pattern only

In this part we analyze $\text{SCM_CTRL_}T_S$ -only, where only the surface temperature varies (moisture can vary but evaporation and environmental q profile scalings are set to 1). This set-up gives the expected rainfall response to the large-scale circulation induced by surface temperature patterns, under the WTG approximation.

$\text{SCM_CTRL_}T_S$ -only precipitation results are shown in Fig. 2a for each surface temperature, and compared with the HG3-AMIP distribution of precipitation over the ocean, for each corresponding SST bin. The qualitative relationship between SST and precipitation is fairly well reproduced in the SCM, but the SCM precipitation is too sensitive to the surface temperature compared with the GCM. This is associated with an overestimation of the sensitivity of the parametrized vertical velocity w' to the surface temperature (Fig. 2b).

There are many possible reasons for the SCM not to perfectly reproduce the GCM rainfall. Our SCM set-up is an idealized model, based on an approximation and with simplified representation of moisture advection. Besides, the WTG approximation is not always accurate, as the free tropo-

spheric temperature is not perfectly uniform across the tropics, particularly outside the equatorial band (10N-10S) and over land regions outside the equatorial band (Todd et al. 2018). On the other hand, its accuracy over land regions within the equatorial band has been shown for the Amazon (Anber et al. 2015). Our SCM set-up is also not meant to capture all the mechanisms that exist in the GCM; only the effect of T_S patterns on the large-scale circulation via convective instability and free-tropospheric heating patterns. However, the most likely reason for the over-sensitivity of w' and precipitation to the surface temperature is the relative isolation and lack of variability of the simulated single column. In the GCM, each column is affected by transients, weather systems, disturbances from nearby columns, that are lacking in the SCM. As it is not disturbed, the vertical velocity in the single column is relatively free to grow or decline, as a consequence of positive feedbacks detailed in Supplementary section 2. As a result, the single column reaches a steady state after a few days, that tends to be either too wet or too dry, even though horizontal mixing of moisture prevents it from getting excessive (see Supp. sec. 2).

Fig. 3b shows SCM_CTRL_ T_S -only precipitation results on a map, projecting it on HG3-AMIP surface temperatures (see Methods). Over the ocean, the precipitation pattern is sensible (correlation over the ocean: 0.7; correlation including land: 0.42). Not surprisingly, it closely follows the SST pattern (not shown), raining over warm regions. As found in other studies, tropical annual mean rainfall can be fairly sensibly reproduced by an SCM under the WTG approximation (Sobel and Bretherton 2000; Zhu and Sobel 2012). Over land, precipitation is generally underestimated, as a result of land regions being relatively cold compared to the tropical average; except over the Sahel, northern Australia and India, which are the hottest regions of the tropics and where precipitation is overestimated.

As mentioned before, this SCM set-up represents the effect of T_S patterns on the large-scale circulation via convective instability and free-tropospheric heating patterns. While this drives most of

the low-level wind convergence in the tropics, other mechanisms have been suggested to dominate in some particular regions, such as regions of strong meridional SST gradients near the equator, and on the flanks of the oceanic Inter-Tropical Convergence Zone (ITCZ) (Chiang et al. 2001; Diakhaté et al. 2018). In particular, in the central-eastern Pacific, boundary-layer pressure gradients driven by the strong meridional SST gradients create low-level wind convergence that forces convection, rather than being a consequence of it (Lindzen and Nigam 1987; Back and Bretherton 2009). Our SCM set-up does not capture this influence of T_S gradients on the large-scale circulation via boundary-layer pressure gradients. This could explain some of the differences between the GCM and the SCM, such as the too-weak and too-wide ITCZ produced by SCM_CTRL- T_S -only in the north-east Pacific (Fig. 3b), and thus support the idea that the effect of T_S gradients plays a key role in this region.

Figure 4a confirms the good correspondence between the SCM and the GCM precipitation over the ocean, as shown by the linear regression of one on another, although the SCM tends to generally overestimate rainfall. In particular, over some oceanic grid-points (blue dots), the annual-mean precipitation is high in the SCM but low in the GCM, which corresponds to SCM overestimations at high SSTs on Fig. 2a. Figure 4a also confirms the lack of correspondence over land, with the SCM raining too much in GCM dry regions, and not enough in GCM rainy regions (given the poor correlation over land, no linear regression is shown).

In the real world, precipitation and SST patterns do not exactly match. One thing in particular that SCM_CTRL- T_S -only is missing is the spatial variation of near-surface and atmospheric moisture. Only one moisture profile was used to define the environment in SCM_CTRL- T_S -only, while moisture is not uniform across the tropics. Variations of moisture are especially an issue for representing relatively cold but wet land regions such as rainforests, or hot but dry land regions

293 such as deserts. In the next section and the rest of this study, the column moisture will be varied
294 (in addition to surface temperature), using SCM_CTRL, to address these issues.

295 *b. Reproduction from surface temperature and relative humidity patterns*

296 From now on we analyze the SCM_CTRL set of experiments (see section 2.c), where not only
297 the surface temperature varies but also moisture, through variations of evaporation and environ-
298 mental q profile scalings. Figure 3c shows SCM_CTRL precipitation results on a map, projecting
299 it on HG3-AMIP T_S and RH_S (see Methods). Considering moisture variation clearly improves the
300 projected rainfall pattern (higher correlation with HG3-AMIP: 0.8 over the ocean and 0.71 includ-
301 ing land). Over land, varying moisture now allows the representation of relatively cold and wet
302 regions like rainforests and hot, dry regions like deserts. In the GCM, RH_S affects precipitation,
303 but precipitation also feeds back on RH_S , so the causality between moisture and rainfall patterns
304 is unclear. In the SCM, the causality is clearer, even though RH_S variations are not directly pre-
305 scribed (but induced by variations in the moisture coefficients), because precipitation has very
306 limited ways of feeding back on to RH_S .

307 But what is the SCM not able to capture? Figure 3d highlights differences with HG3-AMIP
308 precipitation pattern. The sensitivity of precipitation to the surface temperature remains overesti-
309 mated in the SCM. This is consistent with rainfall over the ocean being too extended spatially and
310 generally too strong, while regions with low rain rates are generally too dry. This is also consistent
311 with land regions remaining too dry, except for some rainforests. It remains unclear whether it
312 is due to the SCM parametrization or whether it has a physical explanation such as rainfall being
313 driven by other factors than local surface temperature and humidity. Over land, low thermal iner-
314 tia, consequently strong diurnal cycle, as well as orography or soil moisture play a large role in
315 circulation and convective systems, none of which are directly represented in the SCM. For exam-

316 ple, the mean precipitation over land partly results from the diurnal cycle of surface temperature,
317 which may be very different from the precipitation resulting from the mean surface temperature.
318 Another thing the SCM does not reproduce is the fact that convection over coastal land drives low-
319 level mass divergence over nearby coastal ocean, forcing subsidence and advective drying there,
320 which are not well captured by T_S and moisture patterns. Over the Maritime continent for exam-
321 ple, even though considering moisture heterogeneity and transport allows a better representation
322 of rainfall, the SCM still overestimates oceanic rainfall near the coasts. It is generally the case for
323 African and Asian tropical coasts as well.

324 Figure 4b confirms that the correspondence between the SCM and the GCM precipitation, over
325 both ocean and land, is substantially improved by considering moisture variations. Despite this
326 strong improvement, the SCM still tends to be either too wet or too dry over land, exhibiting two
327 populations of grid-points in GCM rainy regions: one where the SCM remains dry and another one
328 where the SCM overestimates rainfall. Given the existence of these two populations, regressing
329 linearly the SCM rainfall on the GCM rainfall over land would not be sensible. Overall, the
330 SCM still overestimates rainfall over both land and ocean, as further confirmed by the 20N-20S
331 tropically-averaged annual-mean rainfall, which is 4.84 mm/day in the SCM against 4.34 mm/day
332 in the GCM.

333 5. Perturbed climate experiments

334 In the GCM, we choose to decompose the $4\times\text{CO}_2$ forcing into: (1) land warming due to the
335 plant physiological response to $4\times\text{CO}_2$, (2) land warming due to the $4\times\text{CO}_2$ radiative-only effect,
336 (3) effect of the plant physiological response to $4\times\text{CO}_2$ with prescribed T_S over land and ocean,
337 (4) change in the SST pattern, (5) $4\times\text{CO}_2$ radiative-only effect (no plant physiology) with pre-
338 scribed T_S over land and ocean, (6) uniform + 4 K ocean warming. The first three correspond to

339 perturbations in the land surface. The last two correspond to uniform perturbations that strongly
340 affect the atmospheric budget. We use GCM experiments described in section 3 that isolate those
341 different components of the $4\times\text{CO}_2$ forcing. Figure 5a shows the full annual-mean precipitation
342 response to the $4\times\text{CO}_2$ forcing, as given by abrupt $4\times\text{CO}_2$, and Fig. 5b shows the sum of the six
343 components described above. Fig. 5a and Fig. 5b patterns and magnitudes are consistent (correla-
344 tion: 0.78), suggesting that those six components add up nearly linearly and that looking at each
345 one separately can help us to understand the full response.

346 In order to reproduce each forcing component with the SCM, we use the two sets of SCM
347 experiments perturbed with surface warming (SCM_4K) and $4\times\text{CO}_2$ (SCM_4xCO2) described in
348 section 2.c. Note that in these cases, the SCM results are compared with experiments performed
349 with HadGEM2-ES and ACCESS1.0, which use different physical schemes than HadGEM3 (the
350 SCM's parent GCM). At the time of this study, these experiments have not been performed with
351 HadGEM3. Therefore, it is worth keeping in mind that this could cause differences between
352 the GCM experiments and the SCM results. However, we believe this is unlikely to cause major
353 differences, because SCM_CTRL projects very well on both piSST (HadGEM2-ES), with a pattern
354 correlation of 0.68, and AMIP_PL (ACCESS1.0), with a pattern correlation of 0.73 (when applying
355 the same method as in section 4.b and Fig. 3c; not shown)

356 *a. Perturbed land surface*

357 Figure 6 shows annual-mean precipitation changes associated with different forcing compo-
358 nents, as simulated by the GCM (top of each panel) and reproduced by the SCM (bottom of each
359 panel). Plant transpiration weakens in response to increased atmospheric CO_2 , reducing evapo-
360 transpiration and warming the land surface by reducing its cooling capacity (Sellers et al. 1996;
361 Cox et al. 1999; Dong et al. 2009). Land warming induced by this vegetation forcing, when iso-

lated, results in a general rainfall increase over land (Fig. 6a). When land warming is induced by the direct radiative effect of increased atmospheric CO₂, the response is similar (Fig. 6c) although with a smaller magnitude, as the magnitude of land warming is also smaller (land warms by 0.74°C on average when induced by vegetation and by 0.38°C when induced by the radiative CO₂ effect). In both cases, the SCM captures the general rainfall increase over land (Fig. 6b,d), confirming that land warming brings more rainfall over land.

In the case of the vegetation-induced land warming, the SCM reproduces the right magnitudes of rainfall increases (Fig. 6b), despite the strong sensitivity of its precipitation to surface temperatures (shown in the previous section). This is because we take into account RH_S variations, that we reconstruct in the SCM through variations of evaporation and environmental moisture profile (affecting horizontal moisture advection). Land warming is generally associated with reduced RH_S over land (Joshi et al. 2008; O’Gorman and Muller 2010; Simmons et al. 2010; Chadwick et al. 2016; Byrne and O’Gorman 2016), as confirmed by Fig. S8g, making the SCM able to capture land rainfall increases with the right magnitudes. Land warming induced by vegetation also creates a drying patch over the eastern Amazon (Fig. 6a) which is captured by the SCM (Fig. 6b) thanks to the associated RH_S reduction (Fig. S8g). The causality between reduced rainfall and reduced RH_S remains unclear. There are a few other spots of land rainfall decrease (northeastern Brazil, central-eastern Africa, continental southeastern Asia) that the SCM fails to capture. As a result, it overestimates the average land rainfall increase (Fig. S9a).

In the case of the CO₂-induced land warming, the SCM overestimates the land rainfall increase on average (Fig. S9b). Both T_S and RH_S changes are of weak magnitudes, making it difficult to evaluate the sensitivity of the SCM to these changes. The resulting correlation coefficient between the patterns of Fig. 6c and 6d is very weak. Note that the strong rainfall increase over the Sahara

385 is not significant, because there are less than 6 months of the climatological year for which SCM
386 runs correspond to this region and can be projected on it (not shown).

387 As mentioned above, the vegetation response to increased CO₂ reduces evapotranspiration and
388 subsequently warms the surface over land. The effect of land-surface warming, detailed above,
389 can now be switched off by fixing the land surface temperature. This allows us to isolate the
390 effect of reduced evapotranspiration, which is to generally reduce rainfall over land (Fig. 6e).
391 Both the pattern and magnitudes of land rainfall decreases are well captured by the SCM (Fig. 6f,
392 Fig. S9c). This shows that the sensitivity of the SCM precipitation to RH_S is sensible. Note
393 that for this particular projection, we only use variations in evaporation (using β) to reconstruct
394 the RH_S pattern (i.e. we fixed horizontal advection of moisture), simply for more relevance and
395 consistency with the GCM forcing. However, here again the SCM fails to capture a few spots of
396 land rainfall increases (the same as in the land-warming case: northeastern Brasil, central-eastern
397 Africa, continental southeastern Asia). As a result, the average land rainfall decrease is slightly
398 overestimated by the SCM over tropical America and more strongly over Asia and Oceania.

399 Overall, when forcing is applied over land as it is the case here, the SCM does not capture rainfall
400 changes over the ocean, or over some land regions like northeastern Brazil, central-eastern Africa
401 and continental southeastern Asia. This highlights the role of large-scale circulation changes that
402 are independent from local surface changes and cannot be represented by the SCM. Over the
403 eastern Amazon in particular, the crucial role of remotely-driven changes in low-level wind con-
404 vergence, independent from local surface changes, has been shown by Saint-Lu et al. (2019). The
405 SCM results are consistent with this idea that changes in the local surface temperature and evapo-
406 ration do not dominate regional rainfall changes over land everywhere.

407 *b. Perturbed Sea Surface Temperature pattern*

408 Several studies have shown that changes in SST patterns drive most of the changes in rainfall
409 patterns over the tropical oceans (Xie et al. 2010; Ma and Xie 2013; Chadwick et al. 2014; Kent
410 et al. 2015). The pattern of the rainfall response to changes in the SST pattern is well captured by
411 the SCM (correlation: 0.72), especially over the ocean (correlation: 0.77), as shown by Fig. 6g,h.
412 Despite the strong sensitivity of the SCM precipitation to the SST, the magnitude of the rainfall
413 response is also well captured, thanks to the reconstruction of the RH_5 pattern via variations of
414 moisture (not shown). When regressing linearly the SCM precipitation change on the GCM pre-
415 cipitation change over the ocean (Fig. S10), the slope is very close to 1 with an origin very close
416 to 0, confirming the good correspondence in the magnitudes of rainfall changes between the SCM
417 and the GCM.

418 Overall, this result confirms the dominance of the warmer-get-wetter mechanism in the rainfall
419 response to SST pattern changes over the tropical ocean in GCMs. In particular, the local effect
420 of SST pattern change on convective instability appears to dominate over the influence of SST
421 gradients on boundary layer pressure gradients [Lindzen and Nigam (1987) model], as this second
422 effect is not well represented by the SCM.

423 Over land, the rainfall response to SST pattern changes is not well captured by the SCM. This
424 is not surprising, since the GCM land rainfall responds to the change in the SST pattern via the
425 atmosphere, with a top-down forcing—that we attempt to capture in the SCM with a bottom-up
426 forcing (using the surface temperature and relative humidity). Recall that here, unlike for land-
427 surface perturbations, only the ocean surface is prescribed in the GCM. Changes in the SST pattern
428 directly drive circulation changes over land, which are thus not driven by the land surface. In this
429 case, the only way the SCM can capture the GCM land rainfall changes is via their signatures on

the land surface; for example some drying over the Amazon is captured, probably because of the subsequent RH_S reduction.

c. Perturbed atmospheric CO₂

1) CIRCULATION WEAKENING

As shown in previous studies, the atmospheric overturning circulation weakens as a direct response to increased atmospheric CO₂ (Bony et al. 2013; He and Soden 2015; Chadwick et al. 2014). Additional evidence for this is provided by the reduction of the vertically-integrated convective mass flux (positive upward, M_{INT}) simulated by the GCM in response to the 4×CO₂ radiative-only forcing, especially over the ocean (Fig. 7a). Two important hypotheses to explain the CO₂-induced circulation weakening are: (1) reduced radiative cooling, directly due to increased atmospheric CO₂, heats the atmosphere and suppresses convection, reducing the convective mass flux (i.e reduced radiative cooling has to be balanced by reduced convective heating) (Bony et al. 2013), (2) increasing CO₂ warms dry regions (especially the subtropics) more than convective regions, reducing energy transports between ascent and descent regions and slowing down the associated circulation. Merlis (2015) suggested that the troposphere warms more in dry regions than in wet regions because increasing CO₂ reduces radiative cooling more efficiently as there is less absorption overlap with water vapour and clouds. Both hypotheses could be captured by the SCM, as they involve local changes in radiative cooling.

Figure 7a shows the M_{INT} response to the 4×CO₂ radiative-only direct effect, as simulated by the GCM and projected by the SCM, tropically averaged over ocean and over land. Here, we use the set of SCM experiments perturbed with increased atmospheric CO₂ (SCM_4xCO₂; see section 2.c), based on a 4xCO₂-perturbed environment. In order to investigate the direct response of the SCM vertical convective mass flux to the 4×CO₂ forcing, RH_S is left free to respond instead

of being prescribed from the GCM (this is done by keeping the same scaling coefficients for evaporation and moisture as in the reference experiment, see Methods; corresponding maps are given in Fig. S11a,b). Note that there are no T_S changes anyway since the surface is prescribed over land and ocean. When increasing CO_2 , the SCM captures most of the convective mass flux weakening, as expected (Fig. 7a).

On average over land, the circulation weakening is a lot less pronounced than over the ocean in the GCM (Fig 7a). This is because over most land regions except South America, circulation actually strengthens in response to the $4\times\text{CO}_2$ radiative-only forcing in the GCM (Fig. S11a). One possible explanation is that enhanced warming of the atmospheric column over desert regions reinforces monsoon circulations, by increasing land-ocean pressure gradients (Chadwick et al. 2019). This hypothesis is supported by the fact that the SCM does not capture any circulation strengthening over land (Fig. S11b), since it cannot reproduce such a direct atmospheric teleconnection that is not driven by surface warming.

2) RAINFALL RESPONSE

The rainfall response to the $4\times\text{CO}_2$ radiative-only forcing (Fig. 6i) is strongly consistent with the convective mass flux response mentioned above: rainfall decreases over the ocean following the tropical circulation weakening and increases over land, presumably because of enhanced monsoon systems associated with enhanced subtropical tropospheric warming. Over the ocean, the SCM only produces a very weak rainfall decrease over the southern Indian ocean, the western Atlantic and western Pacific and no clear noticeable change over the central-eastern Pacific. This is consistent with the SCM not fully capturing the circulation weakening, as mentioned above. It is also due to RH_S changes over the ocean: in the GCM, RH_S is increased over the ocean by the weakened circulation (Fig. S8a), probably because of moisture building up near the surface; but

476 in the SCM, increased RH_S tends to increase rainfall and counteract the rainfall reduction induced
477 by the circulation weakening. Over land, the rainfall increase is captured by the SCM, thanks to
478 the associated RH_S increase (Fig. S8a).

479 *d. Uniform ocean warming*

480 1) CIRCULATION WEAKENING

481 Previous studies have shown that the overturning circulation is also weakened by global surface
482 warming (Knutson and Manabe 1995; Ma et al. 2012; He et al. 2014; He and Soden 2015). This
483 is consistent with reduced M_{INT} across the whole tropics when a uniform +4 K ocean warming
484 is applied in the GCM (Fig. 7b). This ocean warming-induced circulation weakening is thought
485 to originate from increasing dry static stability ($\partial\theta/\partial z$) in descent regions (Knutson and Manabe
486 1995). When the surface warms by about 4 K, the troposphere warms even more, as dictated
487 by the shape of moist adiabat which is maintained by convection in the tropics. This vertically
488 non-uniform warming increases the dry static stability, which tends to increase dynamical heating
489 ($w\partial\theta/\partial z$). As dynamical heating and radiative cooling balance each other in descent regions, the
490 limited increase in radiative cooling in descent regions limits the increase in dynamical heating
491 and requires a reduction in the vertical motion w . By mass conservation, this weakens the whole
492 overturning circulation. This process does not only involve the direct local response to increased
493 dry static stability, but it also involves changes in mass transport that are not induced by local
494 surface temperature, and are not captured by the WTG/DGW framework. Therefore, the SCM is
495 not able to fully capture it.

496 Figure 7b shows the M_{INT} response to the uniform ocean +4 K warming, as simulated by the
497 GCM and projected by the SCM tropically averaged over ocean and over land. Here, we use the
498 set of SCM experiments perturbed with surface warming (SCM_4K; see section 2.c), based on

499 a +4K-perturbed environment (warmer and moister). In order to investigate the direct response
 500 of the SCM vertical circulation to the uniform ocean + 4 K warming, RH_5 is left free to respond
 501 instead of being prescribed from the GCM (this is done by keeping the same scaling coefficients
 502 for evaporation and moisture as in the reference experiment, see Methods; corresponding maps
 503 are given in Supplementary Figure S11). When warming the surface (SCM_4K) as in p4KSST, the
 504 SCM does not produce any circulation weakening (Fig. 7b), even over the ocean. As mentioned
 505 above, explicit connections between ascent and descent regions are missing in the SCM, making it
 506 unable to fully capture the circulation weakening. The SCM only locally captures the weakening
 507 of subsidence in descent regions, as required by the local balance between dynamical heating and
 508 radiative cooling with increased dry static stability (Supp. Fig. S12). Therefore, our results support
 509 the above mechanism to explain the ocean warming-induced circulation weakening; that is the idea
 510 that it is not a direct local response to increased stability, but to changes in mass transport between
 511 ascent and descent regions that are independent from local surface changes.

512 Over land, the SCM predicts a strong increase in circulation instead of the strong decrease sim-
 513 ulated by the GCM (Fig. 7b). A simple view to explain this result is that it follows enhanced land
 514 warming: with fixed moisture coefficients, the SCM DGW parametrization predicts that rainfall
 515 increases over land since land warms more than the ocean.

516 2) RAINFALL RESPONSE

517 In response to uniform ocean + 4 K warming, precipitation generally increases over the ocean
 518 following the wet-get-wetter mechanism (Chou et al. 2009) as shown in Fig. 6k. The SCM pro-
 519 duces a general rainfall increase over the ocean but strongly overestimates the magnitude (Fig. 6l).
 520 This is consistent with the SCM not capturing the ocean warming-induced circulation weakening,
 521 as mentioned above, that damps the wet-get-wetter response. Besides, our SCM set-up is not able

522 to represent the fact that as precipitation intensifies, it can decrease on its margins due to enhanced
523 advective drying (Chou et al. 2009).

524 As when perturbing SST patterns, ocean warming directly drives circulation changes over land
525 (top-down forcing), which are thus not driven by the land surface (bottom-up forcing) and are not
526 expected to be captured by the SCM. However, ocean warming also indirectly drives land surface
527 warming, with land warming more than the ocean, associated with reduced RH_S (Sutton et al.
528 2007; Joshi et al. 2008; Dong et al. 2009; Lambert et al. 2011), as confirmed by Fig. S8d. Both en-
529 hanced land-surface warming and reduced RH_S constitute a bottom-up forcing on the atmospheric
530 column, which the SCM can capture. In the GCM, rainfall decreases over almost all tropical land
531 in response to uniform ocean warming (Fig. 6k). Some studies suggest that this is caused by the
532 decline of land RH_S (Fasullo 2012; Chadwick 2016; Lambert et al. 2017), in which case the land
533 rainfall decrease would be a response to a bottom-up forcing, reproducible in the SCM.

534 Other studies emphasize the role of remote tropospheric forcing on local rainfall and surface
535 temperature changes (Chiang and Sobel 2002; Joshi et al. 2008; Giannini 2010). Following these
536 ideas, the land rainfall decrease could be driven by a top-down forcing. For example, tropospheric
537 warming over land (transmitted from the ocean by atmospheric waves, consistent with the WTG
538 approximation) could directly suppress convection by stabilizing the column. Atmospheric sta-
539 bility over land cannot be fully diagnosed from the enhanced land warming, because of potential
540 effects of both reduced RH_S and top-down atmospheric connections. Convection is already in-
541 creased over the ocean, as a direct response to ocean warming; so it cannot be increased over land
542 too, owing to mass and energy conservation. It can be viewed as the atmosphere over land being
543 forced to import increased energy from the atmosphere over the ocean, as suggested by Lambert
544 et al. (2011). Since radiative cooling over land can only increase by a limited amount, convection

545 over land ultimately decreases to reduce latent heating and conserve energy. The SCM would not
546 capture such a top-down atmospheric connection.

547 The SCM fails to capture the land rainfall decrease in response to uniform ocean warming
548 (Fig. 6l). Despite reduced land RH_S , the SCM produces the opposite response, with a strong
549 intensification of rainfall over land. This could indicate that the land rainfall decrease is not a
550 response to the bottom-up forcing associated with reduced RH_S ; but to a top-down forcing, as
551 proposed above. However, it could also simply be a result of the SCM precipitation being overly
552 sensitive to surface temperatures, especially given the strong magnitude of the enhanced land-
553 surface warming in this case (not shown). As a result, it is possible that the effect of land-surface
554 warming dominates over the effect of reduced RH_S in the SCM, even if the opposite happens in
555 the GCM. This means that it is possible that the SCM fails to capture a bottom-up forcing, which
556 it is theoretically able to capture, because of its too-strong sensitivity to the surface temperature.

557 We cannot firmly determine the reasons for the SCM failure to reproduce the land rainfall de-
558 crease, but results are very consistent with Chadwick et al. (2019), who used two experiments
559 isolating land-warming only from ocean-warming only. They showed that they did not add up
560 linearly to the full ocean warming experiment, suggesting that forcing the atmosphere with land
561 warming cannot capture the response of land rainfall to ocean warming.

562 6. Conclusions

563 This study uses a Single Column model (SCM) representing the Weak Temperature Gradient
564 (WTG) approximation with the Damped Gravity Wave (DGW) parametrization and implemented
565 with moisture variations, in order to investigate: 1) how much of the present-day mean tropical
566 rainfall and circulation pattern is associated with T_S and RH_S patterns, 2) how much of the change

567 in the mean tropical rainfall pattern is associated with the change in the tropical mean-state envi-
568 ronment and in the T_S and RH_S patterns.

569 Our first result is that most of the present-day mean tropical rainfall and circulation pattern
570 is associated with T_S and RH_S patterns, confirming the relevance of the WTG approximation.
571 We use the SCM to produce a rainfall pattern that is associated with T_S and RH_S patterns. We
572 show that it captures much of the General Circulation Model (GCM) tropical mean rainfall pattern
573 (correlation with HG3-AMIP of 0.71 over the whole tropics and 0.8 when considering only the
574 ocean), although rainfall tends to extend too much spatially over the ocean. Previous studies have
575 also found good correspondences between SCM and GCM rainfall (Sobel and Bretherton 2000;
576 Zhu and Sobel 2012) but here we implement variations of moisture which considerably improve
577 the rainfall representation, especially over land. Despite the overall good correspondence, the
578 SCM precipitation is too sensitive to the surface temperature compared with the GCM. This is
579 probably associated with the lack of variability and transients in the simulated single column,
580 which is specific to SCMs under the WTG approximation. As a result, the SCM overestimates
581 rainfall on average. Rainfall over the ocean is too spatially extended and generally too strong,
582 while regions with low rain rates are too dry. Land regions are too dry, except for some rainforests.

583 Our second result is that the change in the mean tropical rainfall pattern cannot be fully associ-
584 ated with the change in the tropical mean-state environment and in the T_S and RH_S patterns. The
585 SCM does not successfully reproduce the rainfall response to the full CO_2 forcing. In particular,
586 it fails to limit the increase in rainfall over the ocean and to reproduce the rainfall decrease over
587 land that occur when uniformly warming the ocean. This is, at least partly, because of the crucial
588 role of circulation changes that are driven by remote surface changes through atmospheric tele-
589 connections, highlighting the importance of top-down forcing (as opposed to bottom-up forcing).

590 However, the too-strong sensitivity of the SCM precipitation to the surface temperature could also
591 play a role in these misrepresentations.

592 By analysing the differences between the SCM and the GCM, we were able to show that the
593 weakening of the tropical atmospheric overturning circulation, which constrains rainfall changes,
594 is only partly a direct local response to increasing CO_2 : atmospheric teleconnections between as-
595 cent and descent regions, that are independent from local surface changes, play a crucial role. The
596 tropical atmospheric overturning circulation weakens partly as a direct response to the increased
597 atmospheric CO_2 and partly in response to the subsequent tropics-wide surface warming. These
598 two cases (the direct radiative-only effect of $4 \times \text{CO}_2$ and the uniform ocean warming) are repro-
599 duced in the SCM using two different sets of perturbed SCM runs, based on a perturbed RCE
600 environment (either with increased CO_2 or with $+4 \text{ K}$ surface warming). The SCM captures most
601 of the circulation weakening that is due to the direct radiative effect of increased CO_2 . However,
602 it does not capture the circulation weakening that is due to the uniform surface warming. This
603 suggests that it originates from static stability changes in descent regions, and also relies on at-
604 mospheric teleconnections between descent and ascent regions, that are independent from local
605 surface changes (and not fully captured by the SCM). The fact that the SCM does not represent
606 top-down atmospheric teleconnections, which seem to play a key role in weakening the overturn-
607 ing circulation, explains at least part of the misrepresentation of rainfall changes over the ocean
608 (too much rainfall increase in response to ocean warming).

609 Even though the SCM does not successfully reproduce the full rainfall response to the CO_2
610 forcing, it does successfully reproduce the rainfall response to changes in the SST pattern only.
611 We show that the rainfall response to changes in the SST pattern, which is the dominant part of the
612 full rainfall change over the ocean, can be mostly associated with large-scale circulation changes
613 driven by T_S and RH_S patterns, suggesting a dominant role for the local effect of SST pattern

change on convective instability (rather than the influence of SST gradients on boundary-layer pressure gradients).

The rainfall response to vegetation changes caused by the CO_2 increase, which are a dominant component of rainfall changes over tropical forest regions (Betts et al. 2004; Cao et al. 2012; Chadwick et al. 2017) can also be mostly associated with T_S and RH_S pattern changes. The SCM successfully reproduces the rainfall response to vegetation changes caused by the CO_2 increase. It reproduces rainfall increases over land when forced by land warming, rainfall decreases when forced by evaporation weakening, and even some of the Amazon drying that appears in response to land warming induced by vegetation changes. These results are reassuring, as they suggest that rainfall changes can be well diagnosed from changes in T_S and RH_S , when they are forced by perturbations in surface temperature and evaporation patterns. However, when the forcing is applied over land, the SCM does not capture rainfall changes over the ocean or over some land regions. This suggests that changes in the local surface temperature and evaporation do not dominate regional rainfall changes over land everywhere. Remotely-driven changes in low-level wind convergence, independent from local surface changes, can play a crucial role in some tropical land regions.

We cannot exclude the possibility that our SCM set-up, as a simplified representation of the WTG approximation, using an idealized parametrization in a one-dimensional model, biases our results, due to misrepresenting the sensitivity of rainfall to temperature and humidity. The goal of this study was not to perfectly reproduce the mean tropical rainfall pattern and its response to climate change, but to diagnose its drivers and better understand it. Further work is needed to confirm or disprove our hypotheses. To better represent land regions, the SCM could be coupled to a land-surface model. To test our hypothesis on land precipitation decreases, another set-up could be used by connecting a second column to the existing one, which would not be forced at

the surface but coupled to a land-surface model. Finally, our analyses could be replicated using GCM experiments performed with HadGEM3, the SCM's parent GCM, once they are available. Even though circulation weakening, for example, is a quite robust climate change response across models, this would give more confidence on the attribution of the differences between the SCM and the GCM results for climate change.

Acknowledgments. The authors would like to thank Adam Sobel and the two other anonymous reviewers for their comments and suggestions, that helped to substantially improve the quality of the manuscript. The authors thank Duncan Ackerley for producing of the prescribed-land ACCESS simulations, and Peter Good, Hongyan Zhu, Christopher Holloway and Adam Sobel again for helpful advice and discussions. The ACCESS simulations were undertaken with the assistance of the resources from the National Computational Infrastructure (NCI), which is supported by the Australian Government. Data are publicly available from the NCI. Input surface temperature, soil moisture, and deep soil temperatures are also available from the NCI upon request. The relevant doi (and other metadata) for each of the individual experiments can be found in the supporting information attached to Ackerley et al. (2018). The authors thank the JASMIN and CEDA team for making available the JASMIN computing resource Lawrence et al. (2013). This work was supported by the UK Natural Environment Research Council, grant NE/N018486/1. Rob Chadwick was supported by the Newton Fund through the Met Office Climate Science for Service Partnership Brazil (CSSP Brazil).

APPENDIX A

Mathematical formulation of the Damped Gravity Wave parametrization and horizontal advection schemes in the SCM

660 *a. Damped Gravity Wave parametrization*

661 The DGW parametrization consists in providing a solution to the system of momentum, conti-
662 nuity and hydrostatic equations, that maintains weak free-tropospheric temperature gradients.

663 Our formulation of the DGW parametrization follows Kuang (2008), is described in Daleu et al.
664 (2015) and summarized in this section.

665 Considering the decomposition of a variable X into a mean-equilibrated value \bar{X} and a perturba-
666 tion X' , the 2D linearized perturbed equations of momentum, continuity and hydrostatic balance
667 can be written as:

$$\bar{\rho} \partial_t u' = -\partial_x p' - \varepsilon \bar{\rho} u' \quad (\text{A1})$$

$$\partial_x(\bar{\rho} u') + \partial_z(\bar{\rho} w') = 0 \quad (\text{A2})$$

$$\partial_z p' = \bar{\rho} g \frac{T'_v}{\bar{T}_v} \quad (\text{A3})$$

668 Where ε is the mechanical damping of 1 day^{-1} .

669 This system is solved by assuming a solution in the form $T' = \text{Re}(\hat{T} e^{-ikx})$, describing the temper-
670 ature perturbation T' as vanishing with horizontal distance. This solution represents the horizontal
671 propagation of a gravity wave of a single wave number $k=10^{-6} \text{ m}^{-1}$, that maintains horizontal uni-
672 formity. We performed a few SCM runs using $k=2.10^{-6} \text{ m}^{-1}$ (another value used in the literature):
673 it does not make any noticeable difference (not shown).

674 In steady state, injecting this solution in the system yields:

$$\rho^{ref} w' = \int_z \int_z -\frac{k^2}{\varepsilon} \frac{\rho^{ref} g}{T_v^{ref}} T'_v dz^2 \quad (\text{A4})$$

675 In this framework, the vertical motion w' responds to temperature perturbations which horizon-
 676 tally vanish with respects to the WTG approximation by keeping hydrostatic equilibrium, conti-
 677 nuity and momentum conservation.

678 *b. Moisture advection*

679 We parametrize the horizontal advection of moisture from the environment into the simulated
 680 column. We define two terms of advection. The first one is the lateral drawing, describing the
 681 horizontal advection of moisture by the locally parametrized circulation. The second one is the
 682 moisture relaxation, representing the horizontal mixing of moisture through the mean rotational
 683 flow and transient eddies, unrelated to the circulation parametrized in the column. We argue they
 684 represent different processes and can be used together.

685 1) LATERAL DRAWING

686 Following Daleu et al. (2015), horizontal advection of moisture induced by the vertical motion
 687 is defined as the drawing of the reference air into the simulated domain, at each vertical level:

$$\left(\frac{\partial q}{\partial t}\right)_{drawing} = \max\left(\frac{\partial \omega}{\partial p}, 0\right) (q^{ref} - q) \quad (A5)$$

688
 689 where $\max(\partial_p \omega, 0)$ is non zero only if there is convergence into the simulated column.

690 2) HORIZONTAL MIXING

691 Zhu and Sobel (2012) showed that the sensitivity of rainfall to surface temperature was better
 692 represented by relaxing the moisture profile towards the environment. By representing horizontal

693 mixing, this moisture relaxation scheme prevents the simulated domain from getting unrealistically
 694 different from its environment.

695 We implement the following moisture relaxation scheme in our SCM:

$$\left(\frac{\partial q}{\partial t}\right)_{mixing} = \frac{q_{ref} - q}{\tau_q} \quad (\text{A6})$$

696
 697 where τ_q is the relaxation time-scale that we fix to 1 day. In annual mean, tropical surface
 698 waters can remain at approximately the same temperature (+/- 0.2 K) over a distance of the order
 699 of 500 km (not shown). In the SCM, surface winds are fixed at 5 m/s. It would take about 1.15 days
 700 for moisture to be transported by a mean flow of 5 m/s over 500 km. A time-scale of 1 day would
 701 then be typical of horizontal moisture mixing between the simulated domain and a surrounding
 702 environment, that is far enough to be independent of the former (i.e. not under the same regime).

703 APPENDIX B

704 **Methods for the projection of SCM results on a map**

705 To project a set of SCM runs (SCM_CTRL, SCM_4xCO2 or SCM_4K) on the climatology of
 706 a GCM experiment, we consider the GCM surface temperatures (T_S) anomalies to the tropical
 707 average SST (on 20N-20S), and the SCM T_S anomalies to T_s^{RCE} . In most cases, we will also
 708 consider GCM and SCM near-surface relative humidity values (RH_S). SCM results, T_S and RH_S
 709 are always time-means over the last 40 days of the run. Projections are all performed on every
 710 month of the mean annual cycle of the GCM climatology, and then averaged over the year to
 711 obtain the annual-mean projection.

- Projection using GCM T_S (Fig. 3b): on each grid-point, the SCM run that has the closest T_S anomaly is projected.
- Projection using GCM T_S and RH_S (Fig. 3c, 6b,d,h,j,l): on each grid-point, the SCM run that has the closest T_S anomaly and RH_S is projected.
- Projection using GCM T_S , and using the same β and q profile scaling as for a reference projection, i.e. allowing no change in moisture coefficients (Fig. 7): on a reference projection, of a given set of SCM runs (SCM_REF) on T_S and RH_S from a given GCM experiment (GCM_REF), one particular SCM run, that was performed using a unique combination of (T_S , β , q profile scaling), is projected on one particular month and grid-point of GCM_REF. Thus, each grid-point of each month is associated with one value of β (β_{ref}) and one q profile scaling ($q_scaling_{ref}$), that can be stored. The new projection of a set of SCM runs (SCM PERT) on another GCM experiment (GCM_PERT) is then performed doing the following: on each grid-point, the SCM_PERT run that has the closest T_S anomaly and was performed using β_{ref} and $q_scaling_{ref}$ is projected (i.e. the same β and q profile scaling as the SCM_REF run projected on that same month and on that same grid-point of GCM_REF).
- Projection using GCM T_S and RH_S , and using the same q profile scaling as for another projection (Fig. 6f): the projection of a set of SCM runs (SCM_PERT) on a GCM experiment (GCM_PERT) is performed doing the following. On each grid-point, the SCM_PERT run that has the closest T_S anomaly and RH_S , and that was performed using $q_scaling_{ref}$ is projected (i.e. the same q profile scaling as the SCM_REF run projected on that same month and on that same grid-point of GCM_REF). Only β is allowed to be different.

The conditions for projection on each grid-point, when applicable, are that the SCM and the grid-point T_S and RH_S are not different by more than the spatio-temporal standard-deviation of

the GCM T_S and RH_S , respectively (standard deviation of the flattened 12-months \times latitudes \times longitudes array). As a result, it is possible that nothing projects on the grid-point.

References

Ackerley, D., R. Chadwick, D. Dommenges, and P. Petrelli, 2018: An ensemble of AMIP simulations with prescribed land surface temperatures. *Geoscientific Model Development*, **11** (9), 3865–3881, doi:<https://doi.org/10.5194/gmd-11-3865-2018>, URL <https://www.geosci-model-dev.net/11/3865/2018/gmd-11-3865-2018.html>.

Ackerley, D., and D. Dommenges, 2016: Atmosphere-only GCM (ACCESS1.0) simulations with prescribed land surface temperatures. *Geoscientific Model Development*, **9** (6), 2077–2098, doi:<https://doi.org/10.5194/gmd-9-2077-2016>, URL <https://www.geosci-model-dev.net/9/2077/2016/>.

Anber, U., P. Gentile, S. Wang, and A. H. Sobel, 2015: Fog and rain in the Amazon. *Proceedings of the National Academy of Sciences*, **112** (37), 11 473–11 477, doi:[10.1073/pnas.1505077112](https://doi.org/10.1073/pnas.1505077112), URL <https://www.pnas.org/content/112/37/11473>.

Back, L. E., and C. S. Bretherton, 2009: On the Relationship between SST Gradients, Boundary Layer Winds, and Convergence over the Tropical Oceans. *Journal of Climate*, **22** (15), 4182–4196, doi:[10.1175/2009JCLI2392.1](https://doi.org/10.1175/2009JCLI2392.1), URL <https://journals.ametsoc.org/doi/abs/10.1175/2009JCLI2392.1>.

Bergman, J. W., and P. D. Sardeshmukh, 2004: Dynamic Stabilization of Atmospheric Single Column Models. *Journal of Climate*, **17** (5), 1004–1021, doi:[10.1175/1520-0442\(2004\)017\(1004:DSOASC\)2.0.CO;2](https://doi.org/10.1175/1520-0442(2004)017(1004:DSOASC)2.0.CO;2), URL [https://journals.ametsoc.org/doi/abs/10.1175/1520-0442\(2004\)017%3C1004:DSOASC%3E2.0.CO%3B2](https://journals.ametsoc.org/doi/abs/10.1175/1520-0442(2004)017%3C1004:DSOASC%3E2.0.CO%3B2).

757 Betts, R. A., P. M. Cox, M. Collins, P. P. Harris, C. Huntingford, and C. D. Jones, 2004: The role
 758 of ecosystem-atmosphere interactions in simulated Amazonian precipitation decrease and forest
 759 dieback under global climate warming. *Theoretical and Applied Climatology*, **78** (1), 157–175,
 760 doi:10.1007/s00704-004-0050-y, URL <https://doi.org/10.1007/s00704-004-0050-y>.

761 Bi, D., and Coauthors, 2013: The ACCESS Coupled Model: Description, Control Climate
 762 and Evaluation. *Australian Meteorological and Oceanographic Journal*, doi:[https://doi.org/10.](https://doi.org/10.22499/2.6301.004)
 763 22499/2.6301.004, URL <https://publications.csiro.au/rpr/pub?pid=csiro:EP125874>.

764 Bony, S., G. Bellon, D. Klocke, S. Sherwood, S. Fermepin, and S. Denvil, 2013: Robust direct
 765 effect of carbon dioxide on tropical circulation and regional precipitation. *Nature Geoscience*,
 766 **6** (6), 447–451, doi:10.1038/ngeo1799, URL [http://www.nature.com/ngeo/journal/v6/n6/full/](http://www.nature.com/ngeo/journal/v6/n6/full/ngeo1799.html)
 767 ngeo1799.html.

768 Byrne, M. P., and P. A. O’Gorman, 2016: Understanding decreases in land relative humidity with
 769 global warming: conceptual model and GCM simulations. *Journal of Climate*, doi:10.1175/
 770 JCLI-D-16-0351.1, URL <http://journals.ametsoc.org/doi/abs/10.1175/JCLI-D-16-0351.1>.

771 Cao, L., G. Bala, and K. Caldeira, 2012: Climate response to changes in atmospheric carbon
 772 dioxide and solar irradiance on the time scale of days to weeks. *Environmental Research Letters*,
 773 **7** (3), 034 015, doi:10.1088/1748-9326/7/3/034015, URL [http://stacks.iop.org/1748-9326/7/i=](http://stacks.iop.org/1748-9326/7/i=3/a=034015?key=crossref.b4a65cfba7f3fd7d4078736920eed250)
 774 3/a=034015?key=crossref.b4a65cfba7f3fd7d4078736920eed250.

775 Chadwick, R., 2016: Which Aspects of CO2 Forcing and SST Warming Cause Most Uncertainty
 776 in Projections of Tropical Rainfall Change over Land and Ocean? *Journal of Climate*, **29** (7),
 777 2493–2509, doi:10.1175/JCLI-D-15-0777.1, URL [http://journals.ametsoc.org/doi/abs/10.1175/](http://journals.ametsoc.org/doi/abs/10.1175/JCLI-D-15-0777.1)
 778 JCLI-D-15-0777.1.

779 Chadwick, R., D. Ackerley, T. Ogura, and D. Dommenges, 2019: Separating the influences of land
780 warming, the direct CO₂ effect, the plant physiological effect and SST warming on regional
781 precipitation changes. *Journal of Geophysical Research: Atmospheres*, **0 (ja)**, doi:10.1029/
782 2018JD029423, URL <https://agupubs.onlinelibrary.wiley.com/doi/abs/10.1029/2018JD029423>.

783 Chadwick, R., I. Boutle, and G. Martin, 2013: Spatial Patterns of Precipitation Change
784 in CMIP5: Why the Rich Do Not Get Richer in the Tropics. *Journal of Climate*,
785 **26 (11)**, 3803–3822, doi:10.1175/JCLI-D-12-00543.1, URL <http://journals.ametsoc.org/doi/abs/10.1175/JCLI-D-12-00543.1>.

787 Chadwick, R., H. Douville, and C. B. Skinner, 2017: Timeslice experiments for understand-
788 ing regional climate projections: applications to the tropical hydrological cycle and Euro-
789 pean winter circulation. *Climate Dynamics*, 1–19, doi:10.1007/s00382-016-3488-6, URL <https://link.springer.com/article/10.1007/s00382-016-3488-6>.

791 Chadwick, R., P. Good, T. Andrews, and G. Martin, 2014: Surface warming patterns drive trop-
792 ical rainfall pattern responses to CO₂ forcing on all timescales. *Geophysical Research Let-*
793 *ters*, **41 (2)**, 610–615, doi:10.1002/2013GL058504, URL [http://onlinelibrary.wiley.com/doi/10.](http://onlinelibrary.wiley.com/doi/10.1002/2013GL058504/abstract)
794 [1002/2013GL058504/abstract](http://onlinelibrary.wiley.com/doi/10.1002/2013GL058504/abstract).

795 Chadwick, R., P. Good, and K. Willett, 2016: A Simple Moisture Advection Model of Spe-
796 cific Humidity Change over Land in Response to SST Warming. *Journal of Climate*, **29 (21)**,
797 7613–7632, doi:10.1175/JCLI-D-16-0241.1, URL [http://journals.ametsoc.org/doi/abs/10.1175/](http://journals.ametsoc.org/doi/abs/10.1175/JCLI-D-16-0241.1)
798 [JCLI-D-16-0241.1](http://journals.ametsoc.org/doi/abs/10.1175/JCLI-D-16-0241.1).

799 Chiang, J. C. H., and A. H. Sobel, 2002: Tropical Tropospheric Temperature Varia-
800 tions Caused by ENSO and Their Influence on the Remote Tropical Climate. *Jour-*
801 *nal of Climate*, **15 (18)**, 2616–2631, doi:10.1175/1520-0442(2002)015<2616:TTTVCB>

2.0.CO;2, URL [https://journals.ametsoc.org/doi/abs/10.1175/1520-0442\(2002\)015%3C2616%3ATTTVCB%3E2.0.CO%3B2](https://journals.ametsoc.org/doi/abs/10.1175/1520-0442(2002)015%3C2616%3ATTTVCB%3E2.0.CO%3B2).

Chiang, J. C. H., S. E. Zebiak, and M. A. Cane, 2001: Relative Roles of Elevated Heating and Surface Temperature Gradients in Driving Anomalous Surface Winds over Tropical Oceans. *Journal of the Atmospheric Sciences*, **58** (11), 1371–1394, doi:10.1175/1520-0469(2001)058<1371:RROEHA>2.0.CO;2, URL [https://journals.ametsoc.org/doi/abs/10.1175/1520-0469\(2001\)058%3C1371:RROEHA%3E2.0.CO%3B2](https://journals.ametsoc.org/doi/abs/10.1175/1520-0469(2001)058%3C1371:RROEHA%3E2.0.CO%3B2).

Chou, C., J. D. Neelin, C.-A. Chen, and J.-Y. Tu, 2009: Evaluating the Rich-Get-Richer Mechanism in Tropical Precipitation Change under Global Warming. *Journal of Climate*, **22** (8), 1982–2005, doi:10.1175/2008JCLI2471.1, URL <https://journals.ametsoc.org/doi/abs/10.1175/2008JCLI2471.1>.

Collins, M., and Coauthors, 2013: Long-term Climate Change: Projections, Commitments and Irreversibility. *Climate Change 2013: The Physical Science Basis. Contribution of Working Group I to the Fifth Assessment Report of the Intergovernmental Panel on Climate Change [Stocker et al. 2013]*, Cambridge University Press, 1029–1136.

Cox, P. M., R. A. Betts, C. B. Bunton, R. L. H. Essery, P. R. Rowntree, and J. Smith, 1999: The impact of new land surface physics on the GCM simulation of climate and climate sensitivity. *Climate Dynamics*, **15** (3), 183–203, doi:10.1007/s003820050276, URL <https://doi.org/10.1007/s003820050276>.

Daleu, C. L., and Coauthors, 2015: Intercomparison of methods of coupling between convection and large-scale circulation: 1. Comparison over uniform surface conditions: CONVECTION AND LARGE-SCALE DYNAMICS. *Journal of Advances in Modeling Earth Systems*, **7** (4), 1576–1601, doi:10.1002/2015MS000468, URL <http://doi.wiley.com/10.1002/2015MS000468>.

- 825 Diakhaté, M., A. Lazar, G. d. Cotlogon, and A. T. Gaye, 2018: Do SST gradients drive the monthly
826 climatological surface wind convergence over the tropical Atlantic? *International Journal of*
827 *Climatology*, **38 (S1)**, e955–e965, doi:10.1002/joc.5422, URL <https://rmets.onlinelibrary.wiley.com/doi/abs/10.1002/joc.5422>.
828
- 829 Dong, B., J. M. Gregory, and R. T. Sutton, 2009: Understanding LandSea Warming Contrast in
830 Response to Increasing Greenhouse Gases. Part I: Transient Adjustment. *Journal of Climate*,
831 **22 (11)**, 3079–3097, doi:10.1175/2009JCLI2652.1, URL [https://journals.ametsoc.org/doi/abs/](https://journals.ametsoc.org/doi/abs/10.1175/2009JCLI2652.1)
832 [10.1175/2009JCLI2652.1](https://journals.ametsoc.org/doi/abs/10.1175/2009JCLI2652.1).
- 833 Fasullo, J., 2012: A mechanism for land-ocean contrasts in global monsoon trends in a warming
834 climate. *Climate Dynamics*, **39 (5)**, 1137–1147, doi:10.1007/s00382-011-1270-3, URL <https://doi.org/10.1007/s00382-011-1270-3>.
835
- 836 Giannini, A., 2010: Mechanisms of Climate Change in the Semiarid African Sahel: The Local
837 View. *Journal of Climate*, **23 (3)**, 743–756, doi:10.1175/2009JCLI3123.1, URL <https://journals.ametsoc.org/doi/abs/10.1175/2009JCLI3123.1>.
838
- 839 He, J., and B. J. Soden, 2015: Anthropogenic Weakening of the Tropical Circulation: The Rel-
840 ative Roles of Direct CO₂ Forcing and Sea Surface Temperature Change. *Journal of Climate*,
841 **28 (22)**, 8728–8742, doi:10.1175/JCLI-D-15-0205.1, URL <https://journals.ametsoc.org/doi/10.1175/JCLI-D-15-0205.1>.
842
- 843 He, J., B. J. Soden, and B. Kirtman, 2014: The robustness of the atmospheric circulation and
844 precipitation response to future anthropogenic surface warming. *Geophysical Research Letters*,
845 **41 (7)**, 2614–2622, doi:10.1002/2014GL059435, URL <https://agupubs.onlinelibrary.wiley.com/doi/abs/10.1002/2014GL059435>.
846

847 Held, I. M., and B. J. Soden, 2006: Robust Responses of the Hydrological Cycle to Global Warm-
848 ing. *Journal of Climate*, **19** (21), 5686–5699, doi:10.1175/JCLI3990.1, URL [http://journals.](http://journals.ametsoc.org/doi/abs/10.1175/JCLI3990.1)
849 [ametsoc.org/doi/abs/10.1175/JCLI3990.1](http://journals.ametsoc.org/doi/abs/10.1175/JCLI3990.1).

850 Joshi, M. M., J. M. Gregory, M. J. Webb, D. M. H. Sexton, and T. C. Johns, 2008: Mechanisms
851 for the land/sea warming contrast exhibited by simulations of climate change. *Climate Dynam-*
852 *ics*, **30** (5), 455–465, doi:10.1007/s00382-007-0306-1, URL [https://link.springer.com/article/](https://link.springer.com/article/10.1007/s00382-007-0306-1)
853 [10.1007/s00382-007-0306-1](https://link.springer.com/article/10.1007/s00382-007-0306-1).

854 Kent, C., R. Chadwick, and D. P. Rowell, 2015: Understanding Uncertainties in Future Projec-
855 tions of Seasonal Tropical Precipitation. *Journal of Climate*, **28** (11), 4390–4413, doi:10.1175/
856 JCLI-D-14-00613.1, URL <https://journals.ametsoc.org/doi/10.1175/JCLI-D-14-00613.1>.

857 Knutson, T. R., and S. Manabe, 1995: Time-Mean Response over the Tropical Pacific to In-
858 creased CO₂ in a Coupled Ocean-Atmosphere Model. *Journal of Climate*, **8** (9), 2181–2199,
859 doi:10.1175/1520-0442(1995)008<2181:TMROTT>2.0.CO;2, URL [http://journals.ametsoc.org/](http://journals.ametsoc.org/doi/abs/10.1175/1520-0442(1995)008%3C2181:TMROTT%3E2.0.CO;2)
860 [doi/abs/10.1175/1520-0442\(1995\)008%3C2181:TMROTT%3E2.0.CO;2](http://journals.ametsoc.org/doi/abs/10.1175/1520-0442(1995)008%3C2181:TMROTT%3E2.0.CO;2).

861 Knutti, R., and J. Sedlek, 2013: Robustness and uncertainties in the new CMIP5 climate model
862 projections. *Nature Climate Change*, **3** (4), 369–373, doi:10.1038/nclimate1716, URL <https://www.nature.com/articles/nclimate1716>.
863 [/www.nature.com/articles/nclimate1716](https://www.nature.com/articles/nclimate1716).

864 Kuang, Z., 2008: Modeling the Interaction between Cumulus Convection and Linear Gravity
865 Waves Using a Limited-Domain Cloud SystemResolving Model. *Journal of the Atmospheric*
866 *Sciences*, **65** (2), 576–591, doi:10.1175/2007JAS2399.1, URL [http://journals.ametsoc.org/doi/](http://journals.ametsoc.org/doi/abs/10.1175/2007JAS2399.1)
867 [abs/10.1175/2007JAS2399.1](http://journals.ametsoc.org/doi/abs/10.1175/2007JAS2399.1).

- 868 Kuang, Z., 2011: The Wavelength Dependence of the Gross Moist Stability and the Scale Se-
869 lection in the Instability of Column-Integrated Moist Static Energy. *Journal of the Atmospheric*
870 *Sciences*, **68** (1), 61–74, doi:10.1175/2010JAS3591.1, URL [http://journals.ametsoc.org/doi/abs/](http://journals.ametsoc.org/doi/abs/10.1175/2010JAS3591.1)
871 [10.1175/2010JAS3591.1](http://journals.ametsoc.org/doi/abs/10.1175/2010JAS3591.1).
- 872 Lambert, F. H., A. J. Ferraro, and R. Chadwick, 2017: Land-Ocean Shifts in Tropical Precip-
873 itation Linked to Surface Temperature and Humidity Change. *Journal of Climate*, **30** (12),
874 4527–4545, doi:10.1175/JCLI-D-16-0649.1, URL [http://journals.ametsoc.org/doi/abs/10.1175/](http://journals.ametsoc.org/doi/abs/10.1175/JCLI-D-16-0649.1)
875 [JCLI-D-16-0649.1](http://journals.ametsoc.org/doi/abs/10.1175/JCLI-D-16-0649.1).
- 876 Lambert, F. H., M. J. Webb, and M. M. Joshi, 2011: The Relationship between Land-Ocean Sur-
877 face Temperature Contrast and Radiative Forcing. *Journal of Climate*, **24** (13), 3239–3256, doi:
878 [10.1175/2011JCLI3893.1](http://journals.ametsoc.org/doi/abs/10.1175/2011JCLI3893.1), URL <http://journals.ametsoc.org/doi/abs/10.1175/2011JCLI3893.1>.
- 879 Lawrence, B. N., and Coauthors, 2013: Storing and manipulating environmental big data with
880 JASMIN. *2013 IEEE International Conference on Big Data*, 68–75, doi:10.1109/BigData.2013.
881 6691556.
- 882 Lindzen, R. S., and S. Nigam, 1987: On the Role of Sea Surface Temperature Gradi-
883 ents in Forcing Low-Level Winds and Convergence in the Tropics. *Journal of the At-*
884 *mospheric Sciences*, **44** (17), 2418–2436, doi:10.1175/1520-0469(1987)044<2418:OTROSS>
885 2.0.CO;2, URL [http://journals.ametsoc.org/doi/abs/10.1175/1520-0469\(1987\)044%3C2418%](http://journals.ametsoc.org/doi/abs/10.1175/1520-0469(1987)044%3C2418%3AOTROSS%3E2.0.CO%3B2)
886 [3AOTROSS%3E2.0.CO%3B2](http://journals.ametsoc.org/doi/abs/10.1175/1520-0469(1987)044%3C2418%3AOTROSS%3E2.0.CO%3B2).
- 887 Long, S.-M., S.-P. Xie, and W. Liu, 2016: Uncertainty in Tropical Rainfall Projec-
888 tions: Atmospheric Circulation Effect and the Ocean Coupling. *Journal of Climate*,
889 **29** (7), 2671–2687, doi:10.1175/JCLI-D-15-0601.1, URL [https://journals.ametsoc.org/doi/abs/](https://journals.ametsoc.org/doi/abs/10.1175/JCLI-D-15-0601.1)
890 [10.1175/JCLI-D-15-0601.1](https://journals.ametsoc.org/doi/abs/10.1175/JCLI-D-15-0601.1).

- 891 Ma, J., and S.-P. Xie, 2013: Regional Patterns of Sea Surface Temperature Change: A Source
892 of Uncertainty in Future Projections of Precipitation and Atmospheric Circulation. *Journal of*
893 *Climate*, **26 (8)**, 2482–2501, doi:10.1175/JCLI-D-12-00283.1, URL [https://journals.ametsoc.](https://journals.ametsoc.org/doi/abs/10.1175/JCLI-D-12-00283.1)
894 [org/doi/abs/10.1175/JCLI-D-12-00283.1](https://journals.ametsoc.org/doi/abs/10.1175/JCLI-D-12-00283.1).
- 895 Ma, J., S.-P. Xie, and Y. Kosaka, 2012: Mechanisms for Tropical Tropospheric Circulation
896 Change in Response to Global Warming. *Journal of Climate*, **25 (8)**, 2979–2994, doi:10.1175/
897 JCLI-D-11-00048.1, URL <http://journals.ametsoc.org/doi/abs/10.1175/JCLI-D-11-00048.1>.
- 898 Martin, G. M., and Coauthors, 2011: The HadGEM2 family of Met Office Unified Model climate
899 configurations. *Geoscientific Model Development*, **4 (3)**, 723–757, doi:[https://doi.org/10.5194/](https://doi.org/10.5194/gmd-4-723-2011)
900 [gmd-4-723-2011](https://doi.org/10.5194/gmd-4-723-2011), URL <https://www.geosci-model-dev.net/4/723/2011/>.
- 901 Merlis, T. M., 2015: Direct weakening of tropical circulations from masked CO2 radiative forcing.
902 *Proceedings of the National Academy of Sciences*, **112 (43)**, 13 167–13 171, doi:10.1073/pnas.
903 1508268112, URL <http://www.pnas.org/content/112/43/13167>.
- 904 O’Gorman, P. A., and C. J. Muller, 2010: How closely do changes in surface and column water
905 vapor follow Clausius-Clapeyron scaling in climate change simulations? *Environmental Re-*
906 *search Letters*, **5 (2)**, 025 207, doi:10.1088/1748-9326/5/2/025207, URL [http://stacks.iop.org/](http://stacks.iop.org/1748-9326/5/i=2/a=025207)
907 [1748-9326/5/i=2/a=025207](http://stacks.iop.org/1748-9326/5/i=2/a=025207).
- 908 Oueslati, B., S. Bony, C. Risi, and J.-L. Dufresne, 2016: Interpreting the inter-model spread in
909 regional precipitation projections in the tropics: role of surface evaporation and cloud radiative
910 effects. *Climate Dynamics*, **47 (9-10)**, 2801–2815, doi:10.1007/s00382-016-2998-6, URL [https:](https://link.springer.com/article/10.1007/s00382-016-2998-6)
911 [/link.springer.com/article/10.1007/s00382-016-2998-6](https://link.springer.com/article/10.1007/s00382-016-2998-6).

912 Saint-Lu, M., R. Chadwick, F. H. Lambert, and M. Collins, 2019: Surface warming and atmo-
 913 spheric circulation dominate rainfall changes over tropical rainforests under global warming.
 914 *Geophysical Research Letters*, **n/a (n/a)**, doi:10.1029/2019GL085295, URL [https://agupubs.](https://agupubs.onlinelibrary.wiley.com/doi/abs/10.1029/2019GL085295)
 915 [onlinelibrary.wiley.com/doi/abs/10.1029/2019GL085295](https://agupubs.onlinelibrary.wiley.com/doi/abs/10.1029/2019GL085295).

916 Sellers, P. J., and Coauthors, 1996: Comparison of Radiative and Physiological Effects of Doubled
 917 Atmospheric CO₂ on Climate. *Science*, **271 (5254)**, 1402–1406, doi:10.1126/science.271.5254.
 918 1402, URL <http://science.sciencemag.org/content/271/5254/1402>.

919 Shepherd, T. G., 2014: Atmospheric circulation as a source of uncertainty in climate change
 920 projections. *Nature Geoscience*, **7 (10)**, 703–708, doi:10.1038/ngeo2253, URL [https://www.](https://www.nature.com/articles/ngeo2253)
 921 [nature.com/articles/ngeo2253](https://www.nature.com/articles/ngeo2253).

922 Simmons, A. J., K. M. Willett, P. D. Jones, P. W. Thorne, and D. P. Dee, 2010: Low-frequency
 923 variations in surface atmospheric humidity, temperature, and precipitation: Inferences from re-
 924 analyses and monthly gridded observational data sets. *Journal of Geophysical Research: Atmo-*
 925 *spheres*, **115 (D1)**, doi:10.1029/2009JD012442, URL [https://agupubs.onlinelibrary.wiley.com/](https://agupubs.onlinelibrary.wiley.com/doi/abs/10.1029/2009JD012442)
 926 [doi/abs/10.1029/2009JD012442](https://agupubs.onlinelibrary.wiley.com/doi/abs/10.1029/2009JD012442).

927 Sobel, A. H., and G. Bellon, 2009: The Effect of Imposed Drying on Parameterized Deep Con-
 928 vection. *Journal of the Atmospheric Sciences*, **66 (7)**, 2085–2096, doi:10.1175/2008JAS2926.1,
 929 URL <http://journals.ametsoc.org/doi/abs/10.1175/2008JAS2926.1>.

930 Sobel, A. H., G. Bellon, and J. Bacmeister, 2007: Multiple equilibria in a single-column model
 931 of the tropical atmosphere. *Geophysical Research Letters*, **34 (22)**, L22 804, doi:10.1029/
 932 2007GL031320, URL <http://onlinelibrary.wiley.com/doi/10.1029/2007GL031320/abstract>.

933 Sobel, A. H., and C. S. Bretherton, 2000: Modeling Tropical Precipitation in a Single Column.
 934 *Journal of Climate*, **13** (24), 4378–4392, doi:10.1175/1520-0442(2000)013<4378:MTPIAS>
 935 2.0.CO;2, URL [http://journals.ametsoc.org/doi/abs/10.1175/1520-0442\(2000\)013%3C4378%](http://journals.ametsoc.org/doi/abs/10.1175/1520-0442(2000)013%3C4378%3AMTPIAS%3E2.0.CO%3B2)
 936 [3AMTPIAS%3E2.0.CO%3B2](http://journals.ametsoc.org/doi/abs/10.1175/1520-0442(2000)013%3C4378%3AMTPIAS%3E2.0.CO%3B2).

937 Sobel, A. H., J. Nilsson, and L. M. Polvani, 2001: The Weak Temperature Gradi-
 938 ent Approximation and Balanced Tropical Moisture Waves. *Journal of the Atmospheric*
 939 *Sciences*, **58** (23), 3650–3665, doi:10.1175/1520-0469(2001)058<3650:TWTGAA>2.0.CO;2,
 940 URL [http://journals.ametsoc.org/doi/abs/10.1175/1520-0469\(2001\)058%3C3650:TWTGAA%](http://journals.ametsoc.org/doi/abs/10.1175/1520-0469(2001)058%3C3650:TWTGAA%3E2.0.CO%3B2)
 941 [3E2.0.CO%3B2](http://journals.ametsoc.org/doi/abs/10.1175/1520-0469(2001)058%3C3650:TWTGAA%3E2.0.CO%3B2).

942 Sutton, R. T., B. Dong, and J. M. Gregory, 2007: Land/sea warming ratio in response to climate
 943 change: IPCC AR4 model results and comparison with observations. *Geophysical Research*
 944 *Letters*, **34** (2), doi:10.1029/2006GL028164, URL [https://agupubs.onlinelibrary.wiley.com/doi/](https://agupubs.onlinelibrary.wiley.com/doi/abs/10.1029/2006GL028164)
 945 [abs/10.1029/2006GL028164](https://agupubs.onlinelibrary.wiley.com/doi/abs/10.1029/2006GL028164).

946 Todd, A., M. Collins, F. H. Lambert, and R. Chadwick, 2018: Diagnosing ENSO and Global
 947 Warming Tropical Precipitation Shifts Using Surface Relative Humidity and Temperature.
 948 *Journal of Climate*, **31** (4), 1413–1433, doi:10.1175/JCLI-D-17-0354.1, URL [https://journals.](https://journals.ametsoc.org/doi/10.1175/JCLI-D-17-0354.1)
 949 [ametsoc.org/doi/10.1175/JCLI-D-17-0354.1](https://journals.ametsoc.org/doi/10.1175/JCLI-D-17-0354.1).

950 Vecchi, G. A., and B. J. Soden, 2007: Global Warming and the Weakening of the Tropical
 951 Circulation. *Journal of Climate*, **20** (17), 4316–4340, doi:10.1175/JCLI4258.1, URL [http:](http://journals.ametsoc.org/doi/abs/10.1175/JCLI4258.1)
 952 [//journals.ametsoc.org/doi/abs/10.1175/JCLI4258.1](http://journals.ametsoc.org/doi/abs/10.1175/JCLI4258.1).

953 Walters, D., and Coauthors, 2019: The Met Office Unified Model Global Atmosphere 7.0/7.1
 954 and JULES Global Land 7.0 configurations. *Geoscientific Model Development*, **12** (5), 1909–

1963, doi:<https://doi.org/10.5194/gmd-12-1909-2019>, URL <https://www.geosci-model-dev.net/12/1909/2019/gmd-12-1909-2019.html>.

Wang, S., A. H. Sobel, and Z. Kuang, 2013: Cloud-resolving simulation of TOGA-COARE using parameterized large-scale dynamics. *Journal of Geophysical Research: Atmospheres*, **118** (12), 6290–6301, doi:10.1002/jgrd.50510, URL <https://agupubs.onlinelibrary.wiley.com/doi/abs/10.1002/jgrd.50510>.

Xie, S.-P., C. Deser, G. A. Vecchi, J. Ma, H. Teng, and A. T. Wittenberg, 2010: Global Warming Pattern Formation: Sea Surface Temperature and Rainfall*. *Journal of Climate*, **23** (4), 966–986, doi:10.1175/2009JCLI3329.1, URL <http://journals.ametsoc.org/doi/abs/10.1175/2009JCLI3329.1>.

Zhu, H., and A. H. Sobel, 2012: Comparison of a single-column model in weak temperature gradient mode to its parent AGCM. *Quarterly Journal of the Royal Meteorological Society*, **138** (665), 1025–1034, doi:10.1002/qj.967, URL <http://onlinelibrary.wiley.com/doi/10.1002/qj.967/abstract>.

969	LIST OF TABLES	
970	Table 1.	GCM experiments used in this study (either directly analysed or used for their
971		output to perform other experiments). For each experiment: name (in this pa-
972		per), GCM used to perform it, atmospheric CO ₂ forcing, interacting plant phys-
973		iology, SST forcing and land T_S forcing. 47
974	Table 2.	Definition of the different components of the $4\times\text{CO}_2$ forcing from the experi-
975		ments listed in Table 1. 48

976 TABLE 1. GCM experiments used in this study (either directly analysed or used for their output to perform
977 other experiments). For each experiment: name (in this paper), GCM used to perform it, atmospheric CO₂
978 forcing, interacting plant physiology, SST forcing and land T_S forcing.

Name	GCM	CO ₂	Plant physiology	SST	land conditions
HG3-AMIP	HadGEM3	observations 1989-2008	ON	observations 1989-2008	Free
piControl	HadGEM2-ES	pre-industrial	ON	Free	Free
abrupt4×CO ₂	HadGEM2-ES	pre-industrial × 4	ON	Free	Free
piSST	HadGEM2-ES	observations 1979-2008	ON	piControl	Free
p4KSST	HadGEM2-ES	piSST	ON	Uniform 4 K warming from piControl	Free
a4SST	HadGEM2-ES	piSST	ON	abrupt4×CO ₂	Free
AMIP	ACCESS1.0	observations 1979-2008	ON	observations 1979-2008	Free
AMIP_4xCO2tot	ACCESS1.0	AMIP × 4	ON	AMIP	Free
AMIP_4xCO2rad	ACCESS1.0	AMIP × 4	OFF	AMIP	Free
AMIP_PL	ACCESS1.0	AMIP	ON	AMIP	AMIP
AMIP_PL_4xCO2tot	ACCESS1.0	AMIP	ON	AMIP	AMIP_4xCO2tot
AMIP_PL_4xCO2rad	ACCESS1.0	AMIP	OFF	AMIP	AMIP_4xCO2rad
AMIP_4xCO2tot_PL	ACCESS1.0	AMIP × 4	ON	AMIP	AMIP
AMIP_4xCO2rad_PL	ACCESS1.0	AMIP × 4	OFF	AMIP	AMIP

TABLE 2. Definition of the different components of the $4\times\text{CO}_2$ forcing from the experiments listed in Table 1.

Component	Definition
Uniform + 4 K ocean warming	p4KSST - piSST
SST pattern-only	a4SST - p4KSST
Land warming induced by $4\times\text{CO}_2$ radiative-only forcing	AMIP_PL_4xCO2rad - AMIP_PL
Vegetation-only forcing with prescribed land	AMIP_4xCO2tot_PL - AMIP_4xCO2rad_PL
Land warming induced by Vegetation-only forcing	AMIP_PL_4xCO2tot - AMIP_PL_4xCO2rad
$4\times\text{CO}_2$ radiative-only forcing with prescribed land	AMIP_4xCO2rad_PL - AMIP_PL

LIST OF FIGURES

- Fig. 1.** Schematic of the SCM with the DGW parametrization. θ_{ref} and θ are the reference and simulated potential temperatures, respectively. q_{ref} is the reference specific humidity and w' is the parametrized vertical velocity. The dashed red line represents the potential temperature profile once it has been relaxed towards the reference profile, via vertical advection (represented by the thin red arrows) by the parametrized vertical velocity. 51
- Fig. 2.** (Top) Relationship between precipitation and SST in the SCM_CTRL- T_S -only runs (black line) and in the GCM HG3-AMIP (boxes encompass 50% of the values between the 25th and the 75th percentiles, median is plain bold, mean is dashed). Each SCM experiment corresponds to one prescribed surface temperature value and one resulting equilibrated mean precipitation (taken as the time-mean over the last 40 days of the 100 days-long run to keep only the equilibrated period). Error bars are drawn between the 25th and the 75th percentiles of the range of precipitation values occurring during the equilibrated period of the run. In HG3-AMIP, boxes show the distribution of precipitation found for each SST bin, considering all months and all oceanic grid-points of the tropics (20N-20S). Boxes are 0.5 K-wide and correspond to the surface temperature values used in the SCM experiments. (Bottom) Same but for the relationship between vertical velocity at 500 hPa and SST. 52
- Fig. 3.** Annual-mean precipitation in HG3-AMIP and from SCM runs. a) HG3-AMIP annual mean precipitation. b) Projection of SCM_CTRL- T_S -only precipitation results on HG3-AMIP T_S (see Methods). c) Projection of SCM_CTRL precipitation results on HG3-AMIP T_S and RH_S (see Methods). d) Difference between c) and a). Hatched regions are where there are less than 10 months of the climatological year for which SCM runs correspond to the region and can be projected on it. R on the bottom right is the Pearson pattern correlation with a); R(ocean) is computed over the ocean only. 53
- Fig. 4.** SCM against GCM (HG3-AMIP) annual-mean precipitation. a) SCM_CTRL- T_S -only against HG3-AMIP (i.e. precipitation from Fig. 3b plotted against precipitation from Fig. 3a, taken over the whole tropics). b) SCM_CTRL against HG3-AMIP (i.e. precipitation from Fig. 3c plotted against precipitation from Fig. 3a). Orange dots are land grid-points and blue dots are ocean grid-points. Corresponding linear regressions are shown for land (orange) and ocean (blue). The dashed black line shows the $y=x$ one-to-one line. 54
- Fig. 5.** Annual-mean precipitation responses to a combination of forcings in the GCM. a) Fully coupled response to increased atmospheric CO₂: abrupt4×CO₂ - piControl. b) Sum of the responses to six different components of the 4×CO₂ forcing, namely (1) the change in the SST pattern, (2) the land warming due to the 4×CO₂ radiative-only effect, (3) the effect of the plant physiological response to 4×CO₂ with prescribed T_S over land and ocean, (4) the land warming due to the plant physiological response to 4×CO₂, (5) the 4×CO₂ radiative-only effect (no plant physiology) with prescribed T_S over land and ocean, and (6) the uniform + 4 K ocean warming: a4SST - piSST + AMIP_4xCO2tot_PL + AMIP_PL_4xCO2tot - 2*AMIP_PL. R is the Pearson pattern correlation between a) and b). 55
- Fig. 6.** Annual-mean precipitation responses to different components of the 4×CO₂ forcing, in the GCM and from SCM runs. Each panel shows on the top the GCM rainfall response and on the bottom the corresponding SCM projection. When not specified otherwise, projections are done using T_S and RH_S (Methods). Hatched regions are where there are less than 10 months of the climatological year for which SCM runs correspond to the region and can be projected on it (for either one of the two projections compared). R is the Pearson pattern correlation between the SCM projection and the GCM; R(ocean) is when considering the ocean only; R(land) when con-

sidering land only. a) AMIP_PL_4xCO2tot - AMIP_PL_4xCO2rad. b) [Projection of
 SCM_CTRL on AMIP_PL_4xCO2tot] - [proj. of SCM_CTRL on AMIP_PL_4xCO2rad].
 c) AMIP_PL_4xCO2rad - AMIP_PL. d) [Proj. of SCM_CTRL on AMIP_PL_4xCO2rad]
 - [proj. of SCM_CTRL on AMIP_PL]. e) AMIP_4xCO2tot.PL - AMIP_4xCO2rad.PL. f)
 [Proj. of SCM_4xCO2 on AMIP_4xCO2tot.PL, done using T_S and RH_S and using the same
 q profile scaling as for the proj. of SCM_4xCO2 on AMIP_4xCO2rad.PL (so that only evap-
 oration is allowed to change; Methods)] - [proj. of SCM_4xCO2 on AMIP_4xCO2rad.PL].
 g) a4SST - p4KSST. h) [Proj. of SCM_4K on a4SST] - [proj. of SCM_4K on p4KSST].
 i) AMIP_4xCO2rad.PL - AMIP_PL. j) [Proj. of SCM_4xCO2 on AMIP_4xCO2rad.PL] -
 [proj. of SCM_CTRL on AMIP_PL]. k) p4KSST - piSST. l) [Proj. of SCM_4K on p4KSST]
 - [proj. of SCM_CTRL on piSST]. 56

Fig. 7. Annual-mean convective mass flux (positive upward, M_{INT} , left panel) and near-surface rel-
 ative humidity (RH_S , right panel) responses to different components of the $4 \times \text{CO}_2$ forcing,
 in the GCM and from SCM runs. The top and bottom panels correspond to two compo-
 nents of the forcing indicated in the panels titles. Each shows GCM responses (plain bars)
 and corresponding SCM projections (circled-patterned bars) with fixed moisture coefficients
 (details hereafter), averaged over tropical (20N-20S) ocean (blue bars) and land (orange
 bars). a) and c) GCM: AMIP_4xCO2rad.PL - AMIP_PL; SCM: [Projection of SCM_4xCO2
 on AMIP_4xCO2rad.PL, done using T_S only and using the same β and q profile scaling as
 for the projection of SCM_CTRL on AMIP_PL (Methods)] - [projection of SCM_CTRL
 on AMIP_PL (done using T_S and RH_S ; Methods)]. b) and d) GCM: p4KSST - piSST;
 SCM: [Projection of SCM_4K on p4KSST, done using T_S only and using the same β and
 q profile scaling as for the projection of SCM_CTRL on piSST (Methods)] - projection of
 SCM_CTRL on piSST (done using T_S and RH_S ; Methods). 57

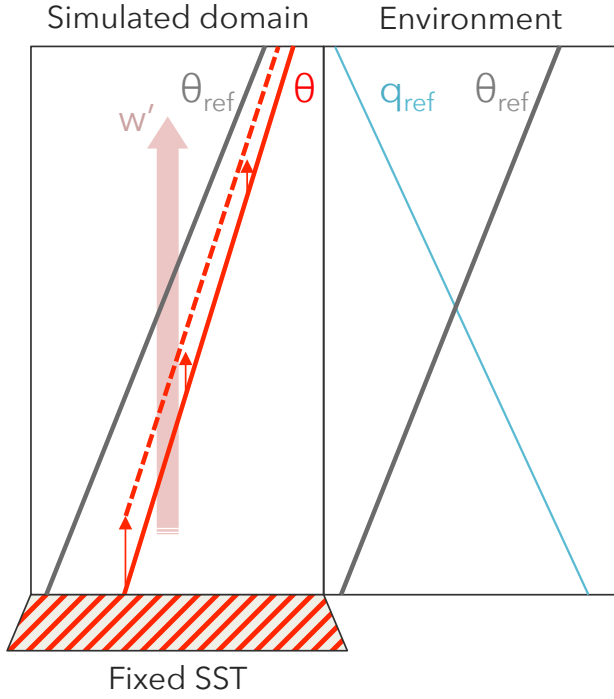
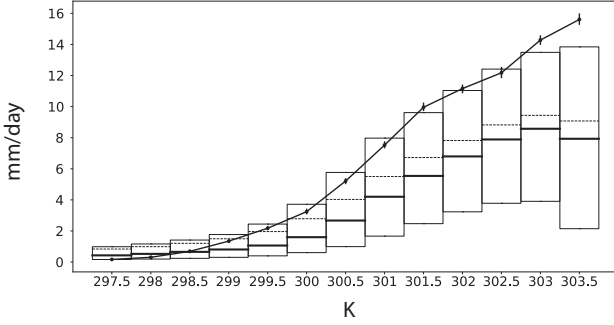


FIG. 1. Schematic of the SCM with the DGW parametrization. θ_{ref} and θ are the reference and simulated potential temperatures, respectively. q_{ref} is the reference specific humidity and w' is the parametrized vertical velocity. The dashed red line represents the potential temperature profile once it has been relaxed towards the reference profile, via vertical advection (represented by the thin red arrows) by the parametrized vertical velocity.

a) Precipitation against SST



b) Vertical velocity at 500 hPa against SST

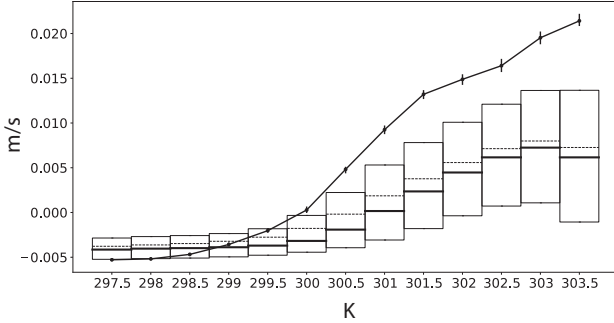


FIG. 2. (Top) Relationship between precipitation and SST in the SCM_CTRL- T_5 -only runs (black line) and in the GCM HG3-AMIP (boxes encompass 50% of the values between the 25th and the 75th percentiles, median is plain bold, mean is dashed). Each SCM experiment corresponds to one prescribed surface temperature value and one resulting equilibrated mean precipitation (taken as the time-mean over the last 40 days of the 100 days-long run to keep only the equilibrated period). Error bars are drawn between the 25th and the 75th percentiles of the range of precipitation values occurring during the equilibrated period of the run. In HG3-AMIP, boxes show the distribution of precipitation found for each SST bin, considering all months and all oceanic grid-points of the tropics (20N-20S). Boxes are 0.5 K-wide and correspond to the surface temperature values used in the SCM experiments. (Bottom) Same but for the relationship between vertical velocity at 500 hPa and SST.

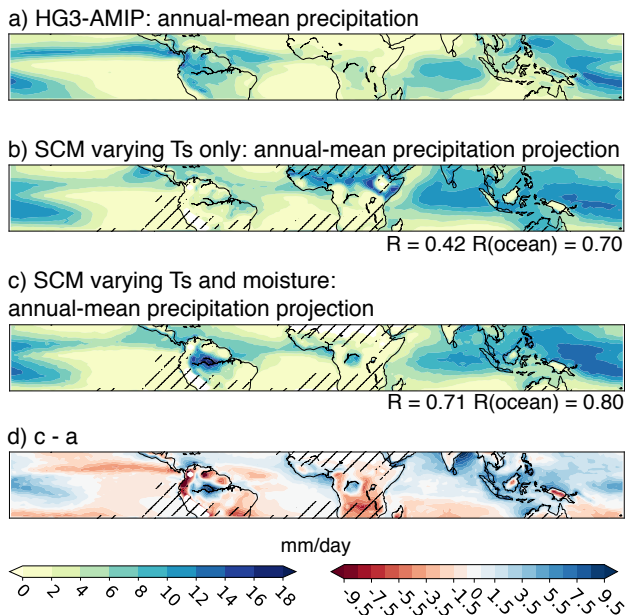


FIG. 3. Annual-mean precipitation in HG3-AMIP and from SCM runs. a) HG3-AMIP annual mean precipitation. b) Projection of SCM_CTRL_ T_s -only precipitation results on HG3-AMIP T_s (see Methods). c) Projection of SCM_CTRL precipitation results on HG3-AMIP T_s and RH_s (see Methods). d) Difference between c) and a). Hatched regions are where there are less than 10 months of the climatological year for which SCM runs correspond to the region and can be projected on it. R on the bottom right is the Pearson pattern correlation with a); R(ocean) is computed over the ocean only.

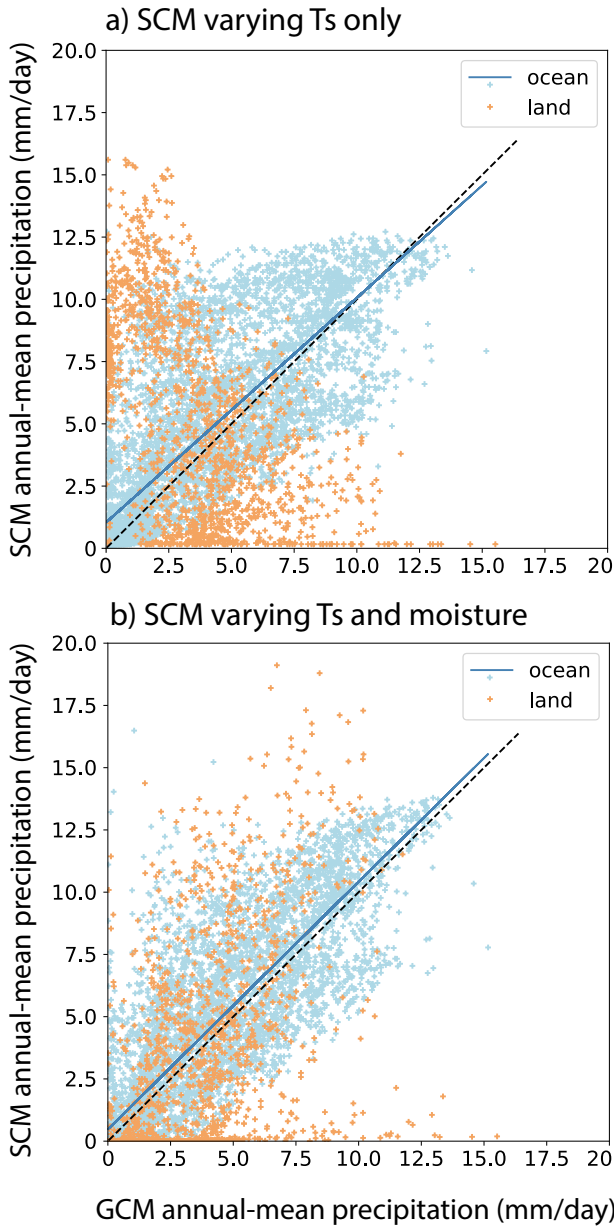


FIG. 4. SCM against GCM (HG3-AMIP) annual-mean precipitation. a) SCM_CTRL_ T_S -only against HG3-AMIP (i.e. precipitation from Fig. 3b plotted against precipitation from Fig. 3a, taken over the whole tropics). b) SCM_CTRL against HG3-AMIP (i.e. precipitation from Fig. 3c plotted against precipitation from Fig. 3a). Orange dots are land grid-points and blue dots are ocean grid-points. Corresponding linear regressions are shown for land (orange) and ocean (blue). The dashed black line shows the $y=x$ one-to-one line.

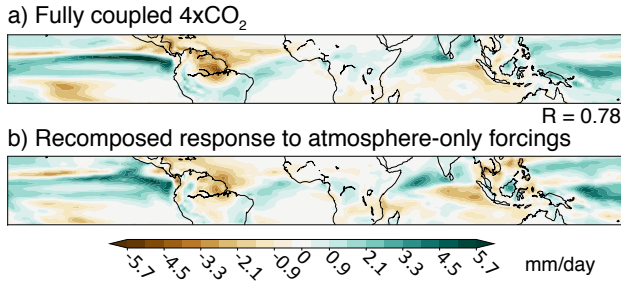


FIG. 5. Annual-mean precipitation responses to a combination of forcings in the GCM. a) Fully coupled response to increased atmospheric CO_2 : abrupt $4\times\text{CO}_2$ - piControl. b) Sum of the responses to six different components of the $4\times\text{CO}_2$ forcing, namely (1) the change in the SST pattern, (2) the land warming due to the $4\times\text{CO}_2$ radiative-only effect, (3) the effect of the plant physiological response to $4\times\text{CO}_2$ with prescribed T_S over land and ocean, (4) the land warming due to the plant physiological response to $4\times\text{CO}_2$, (5) the $4\times\text{CO}_2$ radiative-only effect (no plant physiology) with prescribed T_S over land and ocean, and (6) the uniform +4 K ocean warming: $a4\text{SST} - \text{piSST} + \text{AMIP_}4\times\text{CO2tot_PL} + \text{AMIP_PL_}4\times\text{CO2tot} - 2*\text{AMIP_PL}$. R is the Pearson pattern correlation between a) and b).

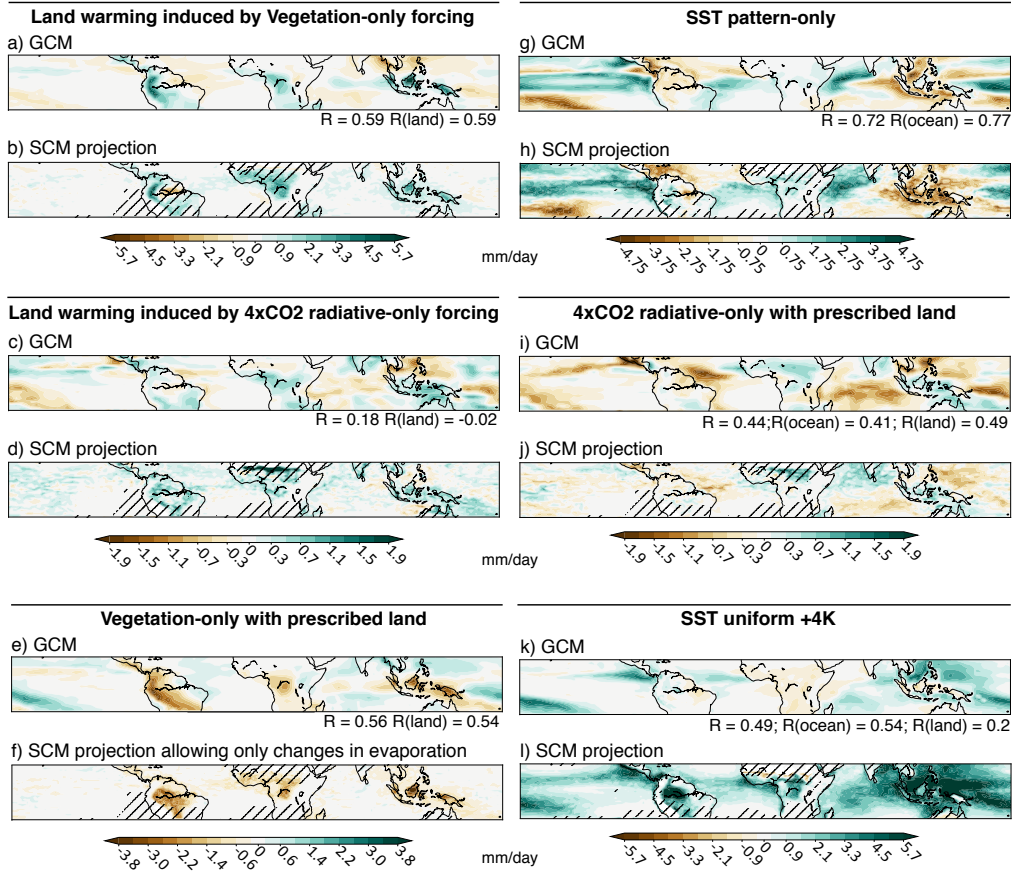


FIG. 6. Annual-mean precipitation responses to different components of the $4\times\text{CO}_2$ forcing, in the GCM and from SCM runs. Each panel shows on the top the GCM rainfall response and on the bottom the corresponding SCM projection. When not specified otherwise, projections are done using T_5 and RH_5 (Methods). Hatched regions are where there are less than 10 months of the climatological year for which SCM runs correspond to the region and can be projected on it (for either one of the two projections compared). R is the Pearson pattern correlation between the SCM projection and the GCM; R(ocean) is when considering the ocean only; R(land) when considering land only. a) AMIP_PL_4xCO2tot - AMIP_PL_4xCO2rad. b) [Proj. of SCM_CTRL on AMIP_PL_4xCO2tot] - [proj. of SCM_CTRL on AMIP_PL_4xCO2rad]. c) AMIP_PL_4xCO2rad - AMIP_PL. d) [Proj. of SCM_CTRL on AMIP_PL_4xCO2rad] - [proj. of SCM_CTRL on AMIP_PL]. e) AMIP_4xCO2tot_PL - AMIP_4xCO2rad_PL. f) [Proj. of SCM_4xCO2 on AMIP_4xCO2tot_PL, done using T_5 and RH_5 and using the same q profile scaling as for the proj. of SCM_4xCO2 on AMIP_4xCO2rad_PL (so that only evaporation is allowed to change; Methods)] - [proj. of SCM_4xCO2 on AMIP_4xCO2rad_PL]. g) a4SST - p4KSST. h) [Proj. of SCM_4K on a4SST] - [proj. of SCM_4K on p4KSST]. i) AMIP_4xCO2rad_PL - AMIP_PL. j) [Proj. of SCM_4xCO2 on AMIP_4xCO2rad_PL] - [proj. of SCM_CTRL on AMIP_PL]. k) p4KSST - piSST. l) [Proj. of SCM_4K on p4KSST] - [proj. of SCM_CTRL on piSST].

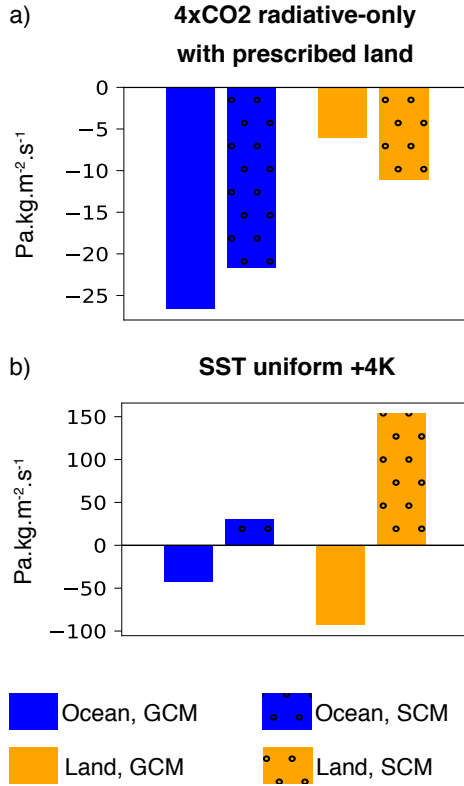


FIG. 7. Annual-mean convective mass flux (positive upward, M_{INT} , left panel) and near-surface relative humidity (RH_S , right panel) responses to different components of the $4\times\text{CO}_2$ forcing, in the GCM and from SCM runs. The top and bottom panels correspond to two components of the forcing indicated in the panels titles. Each shows GCM responses (plain bars) and corresponding SCM projections (circled-patterned bars) with fixed moisture coefficients (details hereafter), averaged over tropical (20N-20S) ocean (blue bars) and land (orange bars). a) and c) GCM: AMIP_4xCO2rad_PL - AMIP_PL; SCM: [Projection of SCM_4xCO2 on AMIP_4xCO2rad_PL, done using T_S only and using the same β and q profile scaling as for the projection of SCM_CTRL on AMIP_PL (Methods)] - [projection of SCM_CTRL on AMIP_PL (done using T_S and RH_S ; Methods)]. b) and d) GCM: p4KSST - piSST; SCM: [Projection of SCM_4K on p4KSST, done using T_S only and using the same β and q profile scaling as for the projection of SCM_CTRL on piSST (Methods)] - projection of SCM_CTRL on piSST (done using T_S and RH_S ; Methods).